Fluoride-Salt-Cooled, High-Temperature Reactor (FHR)White Paper Integrated Research Project (IRP-2) Workshop 2

Materials, Activation, Tritium and Transport (MATT) Group : Status and Path Forward

Panel Members

David Carpenter (MIT)
Kun Chen (SINAP)
Adrien Couet (UW Madison)
Cristian Coutescu (ORNL)
Charles Forsberg (MIT)
Veronique Ghetta (CNRS)
Digby MacDonald (UCB)
Robert Petroski (Terra Power)
Jeffrey Powers (ORNL)
Raluca Scarlat (UW Madison)
Kumar Sridharan (UW Madison)
Gianqiang Wang (SINAP/TMSR)
Guanghua Wang (SINAP)
Jinsuo Zhang (OSU)

Facilitators

Karl Britsch (UW Madison)
Francesco Carotti (UW Madison)
Hsun-Chia Lin (OSU)
Thomas Chrobak (UW Madison)
Ruchi Gakhar (UW Madison)
Nisarg Patel (UW Madison)
Floren Rubio (UNM)
Huali Wu (UW Madison)

Assistants

Kazi Ahmed (UW Madison)
Meredy Brichford (UW Madison)
Ryan Chesser (OSU)
Daniel Curtis (MIT)
William Derdeyn (UW Madison)
William Doniger (UW Madison)
Stephan Lam (MIT)
Michael Laufer (UCB)
Sam McAlpine (MIT)

Mar 2017

Department of Nuclear Engineering and Engineering Physics
University of Wisconsin, Madison

This research is being performed using funding received from the U. S. Department of Energy Office of Nuclear Energy's Nuclear Energy University Programs.

Contents

List of Figures

List of Tables

Executive Summary

This white paper provides a review of the discussions from one of the three active sessions held at the FHR IRP Workshop on: Materials, Activation, Tritium and Transport (MATT). The workshop held was second workshop conducted by University of California, Berkeley (UCB) from April 12-14, 2016, as part of a series of four workshops to be held, to discuss and review technical and licensing issues for fluoride-salt-cooled, high-temperature reactors (FHRs) design, under a U.S. Department of Energy-sponsored Integrated Research Project (IRP-2). IRP-2 is the sequential FHR project funded by Department of Energy (DOE) after the substantial success of IRP-1 (2012-2014), where University of California, Berkeley (UCB); the Massachusetts Institute of Technology (MIT); University of Wisconsin, Madison (UW Madison) and University of New Mexico (UNM); are the participating Universities. The main purpose of the workshop was benchmark definition and review of ongoing efforts within the IRP, and with the broader research community. The MATT working group first met at this workshop. A previous related FHR workshop had been held in 2012, but its focus was narrower, with corrosion studies being primary, tritium as a secondary topic. The current scope of the MATT working group has expanded to include materials, activation products, tritium transport, isotope transport, and salt chemistry and electrochemistry.

This white paper reviews materials-salt interaction and characteristic tritium transport problem unique to FHRs, and discusses existing modeling and experimental basis for FHR technology. The present white paper is derived from the research performed at the participating institutions, and the input and comments of the workshop experts. One major goal of this workshop was to discuss the implementation of best benchmarking practices in the FHR research, with a large amount of discussion centered around tritium [1]. This document is divided into five chapters and the important benchmarking issues are integrated into each chapter. Chapter 1 focuses on discussion of tritium systems modeling. It discusses the mechanisms of tritium generation in the salt and the current work being done to model these phenomena, as well as regulations regarding tritium emissions. Chapter 2 focuses on the tritium separation and control systems required to manage the release of tritium. Chapter **Error! Reference source not found.** focuses on the details, specifications and characterization of various forms of carbon used in the reactor.

Chapter 4 emphasizes the various aspects of salt chemistry and electrochemistry, with a focus on redox control. The Beryllium safety issues, which play a central role in the FHR reactor design, are also discussed in this chapter. Chapter 5 provides a summary of results from the static and dynamic corrosion tests carried out at UW Madison. Section 5.2 discusses the design and construction model of a molten salt thermal convection flow loop at UW Madison for dynamic corrosion tests. At last, the concluding remarks from all the five chapters are presented and the path forward to achieve the goals of IRP-2 are defined.

Preamble

Fluoride-salt-cooled High-temperature Reactors (FHRs)[1] are high-temperature low-pressure reactors that use fluoride salt coolants and the same graphite-matrix coated-particle fuel as high-temperature gas-cooled reactors. Fluoride salts have unique thermo-physical properties compared to other reactor coolants, rendering them potentially attractive as coolants for FHRs. In order to develop the technical basis to design and license commercial FHRs, an integrated research project (IRP-1) was funded by the U.S. Department of Energy (DOE) in January 2012. University of California, Berkeley (UCB); the Massachusetts Institute of Technology (MIT); and University of Wisconsin, Madison (UW Madison); were the three participating institutes. As part of IRP-1, UCB organized a series of four workshops to promote collaboration and discuss the key challenges associated with the FHR research.

A subsequent IRP (IRP-2) was initiated in 2014, which includes University of New Mexico (UNM) along with the three original participating institutes. After substantial success of four workshops of IRP-1, the same approach was continued for IRP-2. Workshop 2 of IRP-2 was conducted by University of California, Berkeley (UCB) from April 12-14, 2016. Experts from around the world were invited to discuss the ongoing research in the field and the related issues with the researchers from partner universities. The workshop was divided into three working groups, each focused on one of the three technical areas:

1. Thermal Hydraulics
2. Neutronics
3. Materials, Activation, Tritium and Transport (MATT)

This white paper presents a summary of discussions and conclusions from the MATT session of Workshop 2 (IRP-2). It covers a variety of topics focused on the materials aspects of FHR research [2].

FHRs are a class of reactor where there are many design choices. The workshop addressed common challenges applicable to most FHRs, not challenges associated with a specific design. The choice of salt depends upon the application but in most cases the base-line coolant is a lithium-beryllium-fluoride salt known as FLiBe ($^7Li_2BeF_4$) primarily because of its thermal hydraulic properties. The characteristics of the FLiBe as well as some of the other potential salts are listed in Table 1.

Table 1. FHR Coolant Options[1]

Coolant	**T_{melt} (°C)**	**T_{boil} (°C)**	**ρ (kg/m^3)**	**ρC_p (kJ/m^3 °C)**
66.7^{7}LiF-33.3BeF$_2$	**459**	**1430**	**1940**	**4670**
59.5 NaF-40.5 ZrF$_4$	500	1290	3140	3670
26 ^{7}LiF-37 NaF-37 ZrF$_4$	436		2790	3500
51 ^{7}LiF-49 ZrF$_4$	509		3090	3750
Water (7.5 MPa)	0	290	732	4040

[1] Compositions in mole percent. Salt properties at 700°C and 1 atmosphere. Water data shown at 290°C and 7.5 MPa for comparison

All proposed salts are multicomponent salts to lower the melting points. The primary coolant system is a closed loop that operates at atmospheric pressure with nominal core coolant inlet and outlet temperatures of 600°C and 700°C, respectively.

The baseline FHR fuel is the graphite-matrix coated-particle fuel developed for High-Temperature Gas-cooled Reactors (HTGRs). Three different fuel configurations have been are proposed by different groups (Figure 1).

- *Pebble bed.* The pebble-bed FHR (PB-FHR) uses 3-cm diameter graphite pebbles with embedded coated-particle fuel—the same basic fuel geometry that was used in the

German HTGRs and will be used in the Chinese HTGRs that are under construction. The pebble-bed design is the most developed of the FHR designs. The reactor is fuelled on-line by circulation of pebbles through the reactor core. Because carbon adsorbs tritium, there is the potential option in this reactor of using the fuel pebbles as a tritium removal system. It is the near-term FHR option.

- *Plate fuel*. Oak Ridge National Laboratory proposed using plate fuel in hexagonal fuel assemblies. The fuel plates are made of a carbon-carbon composite with the coated-particle fuel on the plate surfaces. It is a “traditional” type fuel assembly with a refueling strategy similar to a sodium fast reactor—another low-pressure reactor.
- *Fuel Inside Radial Moderator (FIRM).* This FHR core design uses a fuel configuration somewhat similar to the fourteen operating British Advanced Gas-cooled Reactors (AGRs) except for use of a salt coolant, higher power densities and the details of the fuel design. The AGRs are graphite-moderated carbon-dioxide-cooled high-temperature reactors with gas exit temperatures of 650°C. The AGR fuel consists of UO_2 pellets in stainless steel pins with an assembly consisting of a circular array of pins inside an annular graphite shell. The reactor core is graphite with vertical cylindrical channels that contain the annular fuel assemblies. The FHR FIRM assembly replaces the AGR fuel assembly with a graphite cylinder containing liquid-salt cooling channels and fuel channels filled with coated-particle fuel in carbon-matrix pellets—a cylindrical variant of the prismatic fuel blocks used in some HTGRs.

Pebble Bed

Flat Fuel Plates in Hex Configuration

Fuel Inside Radial Moderator (FIRM)

Figure 1. Alternative FHR Fuel Designs

1 Tritium System-Level Modeling

Tritium systems modeling and tritium management are important to investigate together because they are complementary activities. Tritium systems models inform the community which tritium management system will be most promising, and the experimental work with tritium management concepts feeds back data to validate the tritium system models. This gives system models a more informed output and gives the community more clarity when deciding which management system to pursue. This drives the necessity for analysts and experimentalists to agree on common benchmarks to compare and contrast methods of tritium management. Because this area is relatively undeveloped, this affords quite a bit of freedom in defining these benchmarks.

1.1 Tritium Production

The rate of release is dependent on both the tritium generation and absorption rates. In an FHR, tritium is primarily generated from the constituents of FLiBe by the reactions in Table 1-1. In the FHR, any tritium generated by ternary fission is assumed to be trapped within the fuel pebble. Therefore, all tritium generation is assumed to occur in the salt. As evident in the cross section data, the tritium generation rate depends on the neutron spectrum in the reactor. It also depends on the thermal power of the reactor, the core power density, the initial salt inventory and enrichment, and the core neutron flux. Past molten salt reactor design reports list disparate values for tritium generation rates when normalized by reactor power; see Table 1-2.

Table 1-1. Tritium generation reactions and microscopic cross sections

Reaction	Thermal Cross Section (bn) [3]	One-Group Cross Section for FHR (bn) [4]
${}^{6}_{3}Li + {}^{1}_{0}n \rightarrow {}^{4}_{2}He + {}^{3}_{1}H$	940	148.026
${}^{9}_{4}Be + {}^{1}_{0}n \rightarrow {}^{4}_{2}He + {}^{6}_{2}He$ ${}^{6}_{2}He \rightarrow {}^{4}_{2}He + {}^{6}_{3}Li + {}^{0}_{-1}e + \nu_e$ ($t_{1/2}$ = 0.8 s)	36×10^{-3}	3.63×10^{-3}
${}^{7}_{3}Li + {}^{1}_{0}n \rightarrow {}^{4}_{2}He + {}^{3}_{1}H + {}^{1}_{0}n'$	20×10^{-3}	1.00×10^{-3}
${}^{19}_{9}F + {}^{1}_{0}n \rightarrow {}^{17}_{8}O + {}^{3}_{1}H$	30×10^{-6}	---

Of note is the difference between SS and BOL tritium generation values. Natural lithium is 92.4 mol% Li-7 and 7.6 mol% Li-6. The rate of tritium production from Li-6 is more than four orders of magnitude greater than the rate from any other FLiBe constituent. Therefore, removing Li-6 from natural lithium minimizes tritium production. Even after enriching to 99.995 mol% Li-7, Li-6 contributes greatly to the total tritium generation. At steady state, the MSBR calculations predict that 50% of the tritium will be generated from Li-6 reactions, followed closely by 48% from Li-7 [5]. Calculations for the FHR go as high as 64.4% from Li-6 at steady state [4]. However, Li-6 is also consumed 10^5 times faster than it is produced. As the reactants are consumed, the tritium generation rate falls to a steady state rate 3–10 times lower than the BOL rate. The exponential decay for the Mk 1 FHR is shown in **Error! Reference source not found.**. This result assumes the initial charge of salt is recycled for the duration of the analyzed timeframe. In actuality, salt refreshing would likely occur, but this practice was not incorporated into these results.

Table 1-2. Summary of Molten Salt Reactor Tritium Generation Rates and Relevant Parameters; SS – Steady State, BOL – Beginning of Life

Reactor Type	**MSBR** [5,6]	**MSRE** [5,7]	**AHTR (annular)** [8]	**FHR** [3,9]	**FHTR** [9]	**Mk 1 FHR** [4,10,11]
Tritium Generation Rate (Ci/d) SS/BOL	2420	54	500/5000	32.8	10.2	691/239
Thermal Power (MWt)	2250	7.3	2400	900	100	236
Normalized Tritium Generation Rate (Ci/GWt/d) SS/BOL	**1080**	**7400**	**208.3/ 2083**	**36.4**	**102**	**2931, 10129**
Core Power Density (MWt/m^3)	22.2	3.4	8.3	---	---	22.7
Salt Inventory (m^3) Core/Total	30.41/48.7	0.566	---	---/15	0.456	11.67/ 46.82
Li-7 Enrichment (mol%)	99.995	99.99	99.99	99.995	99.99	99.995
Total Neutron Flux (n/cm^2/s)	2.6×10^{14}	1.5×10^{13}	---	---	2.85×10^{14}	3.41×10^{14}

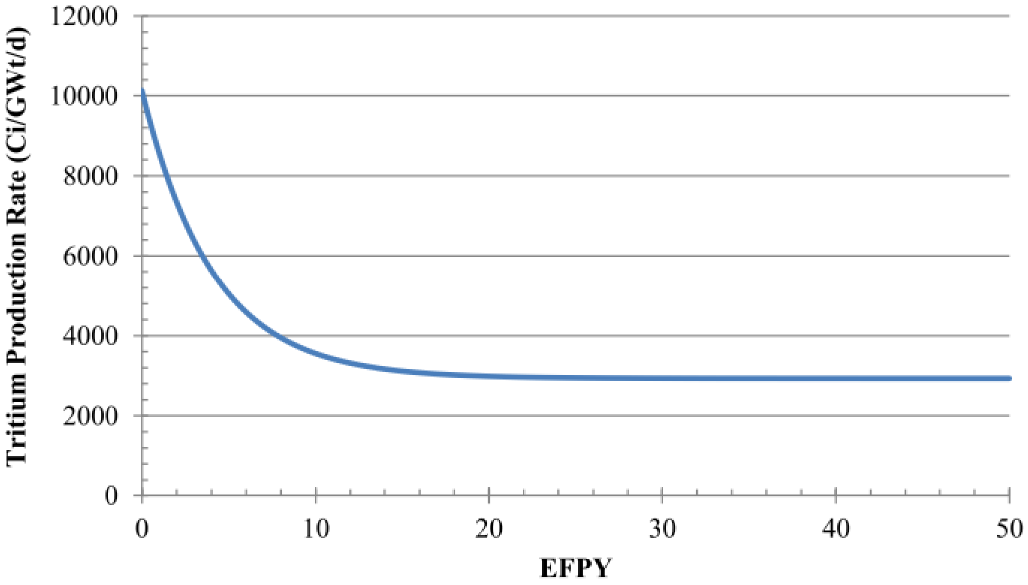

Figure 1-1. Tritium production rate for Mk 1 FHR as a function of time of operation [11]

It should also be noted that both the MSBR and MSRE were fluid-fuel reactors, while the others use solid-fuel. Furthermore, the MSRE data is experimental, while the others are all values expected from calculations. Therefore, these MSRE values incorporate tritium absorption in graphite. Tritium release rates will be lower than generation rates because of this absorption. The tritium-graphite system is discussed in Section 3.4.

In the United States, the regulations surrounding reactor design are given by Sherman and Adams in Table 1-3. The effluent streams shown in Table 1-3 indicate that the limit is based on concentrations of $1x10^{-7}$ μCi/mL in air and $1x10^{-3}$ μCi/mL in water, which will be based on the effluent flow rates and stream dilution used in the FHR power cycle.

Table 1-3. Regulatory limits on tritium emissions in the United States [12]

		Annual Radiation Dose		**Effluent Concentration**			
	Regulation	**mrem**	**mSv**	**Air**		**Water**	
				µCi/mL	**Bq/mL**	**µCi/mL**	**Bq/mL**
Limit	10 CFR 20.1301(a)1	100	1	-	-	-	-
	Table 2 of Appendix B to 10 CFR 20	50	0.5	1x10^{-7}	3.7x10^{-3}	1x10^{-3}	37
Standard	10 CFR 20.1201(e)	25	0.25	(5x10^{-8})[a]	(1.85x10^{-3})[a]	(5x10^{-4})[a]	(18.5)[a]
ALARA	Appendix I to 10 CFR 50	20 (β,air)	0.20	(4x10^{-8})[a]	(1.48x10^{-3})[a]	-	-
		3 (water)	0.03	-	-	1.5x1^{-5}	0.56
Drinking Water	EPA standard	4	0.04	-	-	2x10^{-5}	0.74

a. Calculated by assuming the linear relationship between the annual dose of 50 mrem and the values in Table 2 of Appendix B of 10 CFR 20.
ALARA = as low as reasonably achievable
CFR = Code of Federal Regulations

While no absolute value of radioactive release is mandated, a reasonable emission target could be based on existing licensed reactors. For different reactor types, the total escape is shown in Table 1-4.

Table 1-4. Tritium release rates for different reactor types [11,13]

	Gaseous Effluent*	**Liquid Effluent***	**Total Tritium Escape***
BWR	0.04	0.09	**0.13**
PWR	0.09	0.65	**0.74**
GCR	0.22	0.33	**0.56**
HWR	16.05	4.01	**20.07**

*Units: Ci/GWt/EFPD

In comparison, for an FHR where the release of tritium is unmitigated, the equilibrium value of release (post saturation of structural components) is calculated in TRIDENT to be 2931 Ci/GWt/d, highlighting the imperative for an efficient capture and control system.

1.2 Modeling Tools and Ongoing Development Work

1.2.1 TRIDENT

The system-level model created by John Stempien [11,14] in 2015 named TRItium Diffusion EvolutioN and Transport (TRIDENT) is currently the primary model in use at MIT. Written in MATLAB, TRIDENT is a time-dependent model which accounts for the integrated effects of tritium speciation (T_2 or TF) based on salt chemistry, generation and consumption through corrosion reactions, and tritium diffusion through walls and structures. The summary of tritium flows in the FHR system modeled by TRIDENT are shown in Figure 1-2.

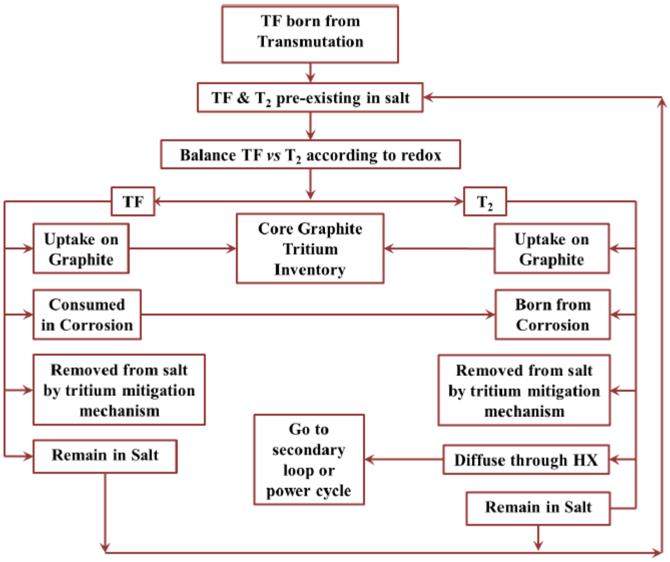

Figure 1-2. TRIDENT Tritium Flow Summary

As shown in Figure 1-2, TRIDENT includes the capability to model tritium removal technologies within the system such as a carbon adsorber bed, permeation window or gas stripping column. Standard configurations for each of these technologies have been previously modeled in TRIDENT and each show potential to significantly reduce peak release rates for a 236 MWt FHR from 2410 Ci/EFPD to ranges around 400-600 Ci/EFPD [14]. Each of these technologies can and need to be further improved through adjustments in size, surface area and use of advanced technologies, such as the combination of ultransonic enhancement in gas sparging outlined in Section 0 or the use of alternative carbon materials in adsorber beds.

While some aspects of this model have been benchmarked against small diffusion experiments by Fukada [15] and corrosion loop experiments at Oak Ridge [16] and show reasonable agreement [11], there is still a significant amount of verification and validation that must be completed. This work includes acquiring experimental data for determination of transport coefficients in system components, which is currently underway at MIT [17].

The TRIDENT code is continually under-development, particularly with respect to individual modules (such as mitigation units). An example of a recent change includes spatial discretization of a carbon adsorber bed and changing from a fixed bed to counter-current bed configuration, which provided incremental performance improvements.

1.2.2 **COMSOL Multiphysics**

COMSOL MultiPhysics provides capability to perform detailed modeling and is currently being investigated for use on the carbon adsorber bed by MIT. COMSOL can be used for 3-D multi-scale modeling, first on the level of a single carbon/graphite pebble, and then on the level of the whole packed bed. Through microscale modeling of a single fuel or adsorbent pebble, insight on the surface and internal usage can be gained. For the purpose of a tower design, spatial homogenization of pebbles must be performed for the full bed to be simulated. As such, modeling exercises should be complete to show that there is decent agreement between microscale and homogenized models and a decent approximation can be achieved. COMSOL will allow for quick tests and sensitivity analyses to optimize mitigation mechanisms outside of the TRIDENT simulation window. If required, COMSOL may be integrated with TRIDENT through LiveLink^{TM} for MATLAB.

Work in progress at UW Madison includes the use of COMSOL to develop a tritium distribution map within the FHR core using heat transfer, fluid flow, and species transport physics. Overall tritium release rates can be benchmarked against TRIDENT and its benchmarks. The COMSOL model will also offer core-level results, which have not previously been studied. Also at UW Madison, COMSOL is used to model tritium transport at the fuel-element level, for steady state conditions and thermal and power transients related to start-up, shut-down, and accident scenarios.

1.2.3 System Analysis Module

System-level analysis of nuclear reactors is important for studying transients with long time-scales. Currently, the group at UW Madison working with Argonne National Laboratory (ANL) to test and develop their System Analysis Module (SAM) code for analysis of molten-salt and salt-cooled reactors. One primary objective is to develop the capability to simulate overcooling (coolant freezing) transients. Overcooling is a potential hindrance to natural circulation coolant flow during scenarios requiring passive decay heat removal. A tritium transport model could be formulated for use in SAM, for investigation of the phenomena coupled with other transients [18]. Because SAM is built on the Multiphysics Object Oriented Simulation Environment (MOOSE) finite-element framework, tritium transport phenomena would be readily coupled to existing thermal hydraulics models in SAM.

1.3 Conclusions

Modeling of tritium transport in the FHR core relies on tritium production rates, which vary drastically based on the design of the core. The flux profile, salt composition, and neutron spectrum, which determines the cross sections, are used to calculate the tritium production rate. Diffusion of tritium into graphite constituents of the core must be understood as a sink for tritium and a source-term for tritium in the event of a temperature transient that might cause its release. Tritium generation and graphite absorption must be modeled to ensure that tritium release quantities comply with U.S. federal regulations. TRIDENT and COMSOL models predict the tritium production and transport phenomena. Modeling of transport phenomena is benchmarked against experimental diffusion data from fusion and previous MSR applications; comparing the results of the FHR-specific codes will also serve as verification.

2 Tritium Separation and Control Systems

Tritium separation and management methods that are being studied include inert gas sparging, tritium solid getters (other than graphite), permeators, carbon, and tritium barriers. These are discussed in this section. Experimental activities in these areas are being performed at UNM, The Ohio State University (OSU), UW Madison, Oak Ridge National Laboratory (ORNL), Shanghai Institute of Applied Physics (SINAP), and The French National Center for Scientific Research (CNRS) in France. Absorption of tritium on carbon is discussed in Section 40. Carbon, including graphite, has multiple roles in the FHR including the neutron moderator in the reactor core, a tritium sink in the reactor core, and potentially a tritium removal technology in external to the reactor core beds.

2.1 Tritium Separation Methods

The leakage of tritium in FHRs is a critical issue for future licensing because it can permeate through piping and heat exchangers and eventually release to the environment. It is estimated that FHRs produce several orders of magnitude more tritium than PWRs [3]. Methods for removing tritium from the flow system include gas sparging, tritium getters, double-wall heat exchangers and tritium barriers. The theory behind these methods is detailed in the following sections.

2.1.1 Gas Sparging

Inert gas sparging was investigated for tritium and fission product removal during MSRE and MSBR projects [19–21]. This technique appears to be an effective method of gas removal from the fuel salt. Because of the past success in the MSRE project and the fact that the FHR uses the same salt (FLiBe), this technique would be a potentially viable method of tritium removal and sequestration for the FHR.

Taking the techniques pioneered by the MSRE project in inert gas sparging [22–24], the University of New Mexico is investigating the enhancement of inert gas sparging by utilizing high powered ultrasonics to increase the gas removal efficiency of inert gas sparging. A prototypical experiment has been constructed to compare the performance of inert gas sparging and ultrasonically inert gas sparging that increases the gas-liquid interface area.

The experiment is shown in Figure 2-1 and is a scaled experiment designed to simulate FLiBe and tritium by using a water/glycerol mixture and dissolved oxygen (DO) as a surrogate. It consists of a pump, bubble injector, test section, bubble separator, and a cooler. The water/glycerol mixture matches the mass transfer non-dimensional numbers of FLiBe at FHR operating temperatures. The concentrations used and their corresponding Schmidt numbers are shown in Table 2-1. The ultrasonic enhancement is provided by an ultrasonic horn placed in the test section as shown in Figure 2-1(b). The loop operates by saturating the fluid with oxygen and uses a sparging gas, argon, to reduce the DO concentration. Sparging is performed with and without ultrasonics. The sparging will be enhanced by an increase in the convective mass transfer by agitation of the bubbles and by the breakup of larger bubbles into smaller bubbles which effectively increases the surface to volume ratio of the two phases.

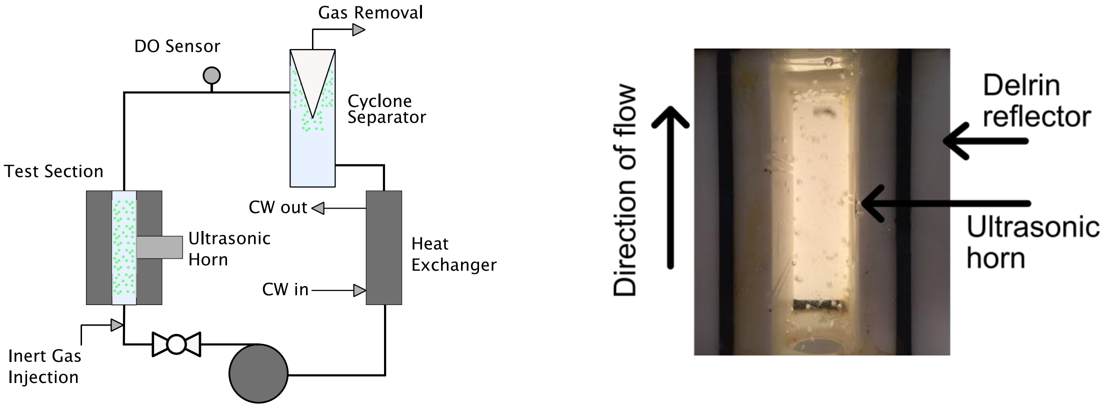

(a) (b)

Figure 2-1. (a) shows the schematic of the prototype flow cell, and (b) shows the flow through the test section.

Table 2-1. Glycerol concentrations used, which correspond with the operating temperature of the MSRE [22]

Concentration (%wt Glycerol)	**Sc**
0	419
12.5	370
25	750
37.5	2015
50	3446

The preliminary results show a large improvement in stripping performance between the inert gas sparging and the enhanced sparging runs. The stripping operation starts from oxygen saturation to a concentration of 3.0 mg/L. Because the saturation of oxygen varies with glycerol concentration, the results were uniformly reported from 8.0 mg/L except for the 50% wt. glycerol, where the starting concentration is 7.0 mg/L. As expected, the visual data does show the breakup of larger bubbles and the general agitation of the sparging bubbles. The DO results for water, as shown in Figure 2-2, show a definite improvement in sparging time. This time reduction was found for concentrations shown in Table 2-1, and the results are shown in Figure 2-3. The preliminary results show that there is a significant time improvement for DO removal between glycerol concentrations of 0 wt. % to 37.5 wt%.

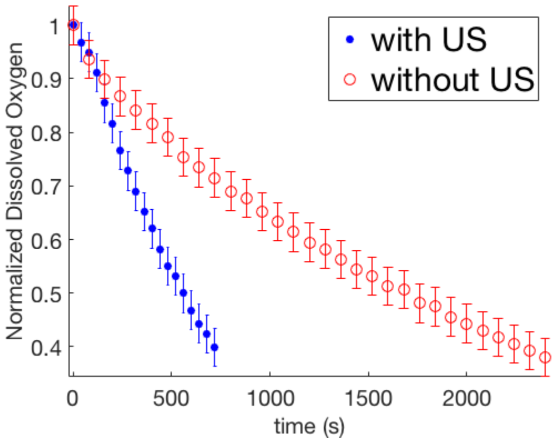

Figure 2-2. Preliminary results from the prototypical flow cell experiment

This experiment was a prototype small-scale water loop with a volume of 0.8 gallon, water volume flowrate of 1.25 GPM, argon flowrate of 0.2 sfcm/min, and intensity of 275 W/cm^2. This shows a reduction in oxygen removal time by about 70%.

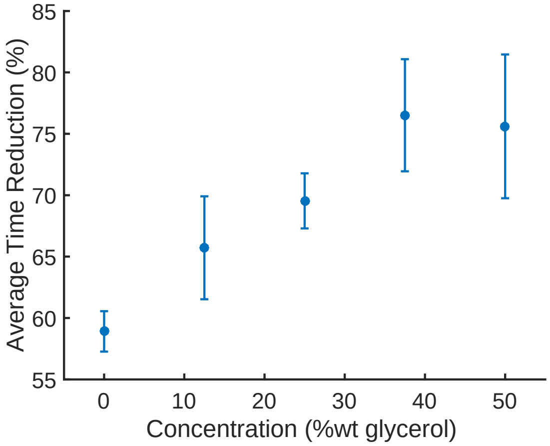

Figure 2-3. Preliminary results from the prototypical flow cell experiment

This shows the reduction in time between ultrasonic and non-ultrasonic run over different concentrations of glycerol. The points are the average of at least three runs at a given concentration of glycerol. (Note: 50% wt was calculated from 7.0 mg/L to 3 mg/L instead of 8.0 mg/L due to oxygen saturation limits). The results from this experiment show potential for increasing the efficacy of inert gas sparging for tritium removal. Applying this technology to a salt purification can significantly decrease the system size and stripping gas necessary to reduce tritium levels to acceptable levels. But, there are still some challenges to address. In this experiment, the ultrasonic horn is in contact with the working fluid. This is not desired for salt purity and radiological reasons because the ultrasonic probe will erode and deposit probe material into the reactor FLiBe. Future experiments will address this by investigating indirect sonication methods. The other challenge is addressing the scale up considerations for applying this prototypical technique to a full scale FHR.

2.1.2 **Double-Wall Heat Exchangers**

Due to high temperatures and large surface of heat exchangers, the amount of tritium leaking from heat exchangers could be unacceptable. Therefore, it is necessary to design innovative heat exchangers that can reduce tritium leakage and maintain good thermal performance simultaneously. Double-wall or “double containment” tubing has been used in many applications in which the mixing of multiple fluids must be avoided. A double-wall twisted-tube heat exchanger for the FHR is being designed and optimized for its heat transfer and minimal tritium release performance [25]. UNM has proposed an intermediate heat exchanger design of a double-wall twisted-tube shell and tube heat exchanger. This investigation will combine modeling and experimental efforts to evaluate the performance of the heat exchanger. RELAP5-3D or another modeling program will be used to computationally quantify and optimize the design of the heat exchanger. Additionally, the double-wall tubing allows for several options to suppress the permeation of tritium through the walls of the heat exchanger [26]. As part of our considerations, we will investigate the increased effectiveness of twisted-tube designs in transferring heat as well as assess the losses a double-wall will have on the heat transfer performance of the exchanger [27].

Both the fission and fusion communities are investigating materials to prevent tritium from migrating through reactor materials. There has been a significant amount of work done in studying barrier coatings and finish options for use on metallic surfaces. While preventing the tritium from permeating to the secondary fluid, a barrier will provide added thermal resistance thus reducing the effectiveness of the heat exchanger.

Another option would be to use a double wall design in pipes or a heat exchanger and fill the intermediate annulus with a gap fluid or sweep gas. A simple flow diagram of the double-wall heat exchanger with sweep gas is shown in Figure 2-4 and compared to one with a tritium getter, described below. To achieve good thermal performance, helium is most likely to be used for its superior thermal conductivity compared with other inert gases. Both fluoride salt and air flow upward and sweep gas flows downward in the annulus simultaneously. The countercurrent flow between two adjacent fluids further enhances heat transfer.

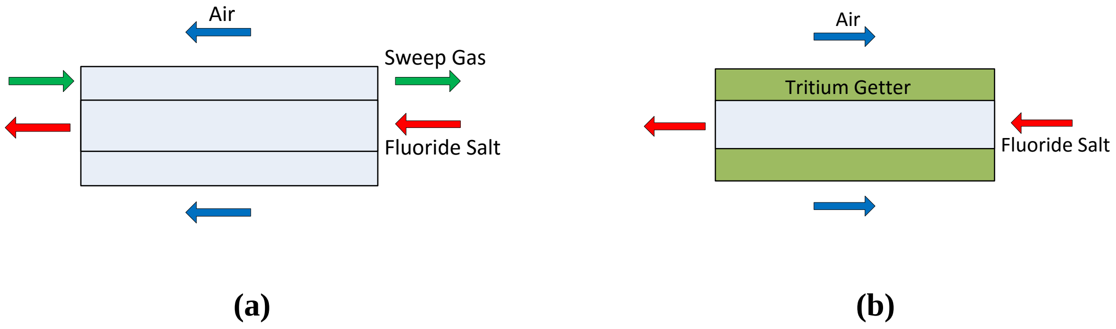

Figure 2-4. Double wall heat exchanger with (a) sweep gas and (b) tritium getter

Filling the intermediate annulus with a hydriding material could be a viable tritium management method for double wall heat exchangers. When exposed to hydrogen and its isotopes, hydriding materials are able to store hydrogen rapidly and reversibly [28]. UNM has proposed to use yttrium hydride to fill the space between tubes in double tube heat exchangers. In a partnership with Los Alamos National Laboratory (LANL), UNM will be performing tests on yttrium hydride investigating its thermal and hydriding properties using the geometry of double-tube heat exchanger. The physical geometry of the hydride is yet to be determined. The final form factor can possibility be a being dust-like, a pebble bed, or solidly filling the annulus. This option provides the ability to remove tritium from the coolant system and store it. Any combination of these options may prove to be ideal, allowing for creativity in our investigation.

The double-wall heat exchanger with sweep gas is being considered for the design of a natural draft heat exchanger (NDHX). The following four tubing designs will be considered: double plain tubes, double fluted tubes, inner plain tubes with outer fluted tubes, and outer plain tubes with inner fluted tubes. A one-dimensional heat and mass transfer model has been proposed and is planned to be used to predict the heat transfer rate and temperature profile of fluids in the inner and outer tubes. The coupled model has been benchmarked using ANSYS Fluent, a Computational Fluid Dynamics (CFD) tool. Figure 2-5 shows a comparison of the fluid temperature profiles. Tube length of the NDHX is normalized to 1. The entrance and exit location of the fluid in the NDHX are annotated as z=0 and z=1, respectively. Fluoride salt flows upward (from right to left in Figure 2-4) without a noticeable temperature decrease. However, sweep gas flows downward (from left to right in Figure 2-4) with a dramatic temperature increase. Air temperature increases rapidly from room temperature (293 K) to fluoride salt temperature (~873 K). Little temperature difference in the tube center region (z=0.6~0.9) means little heat transfer between fluids. Such regions should be eliminated in a heat exchanger, but it is acceptable for code benchmarking purposes. The good agreement of the simulation results indicates that the in-house code can sufficiently predict NDHX thermal performance.

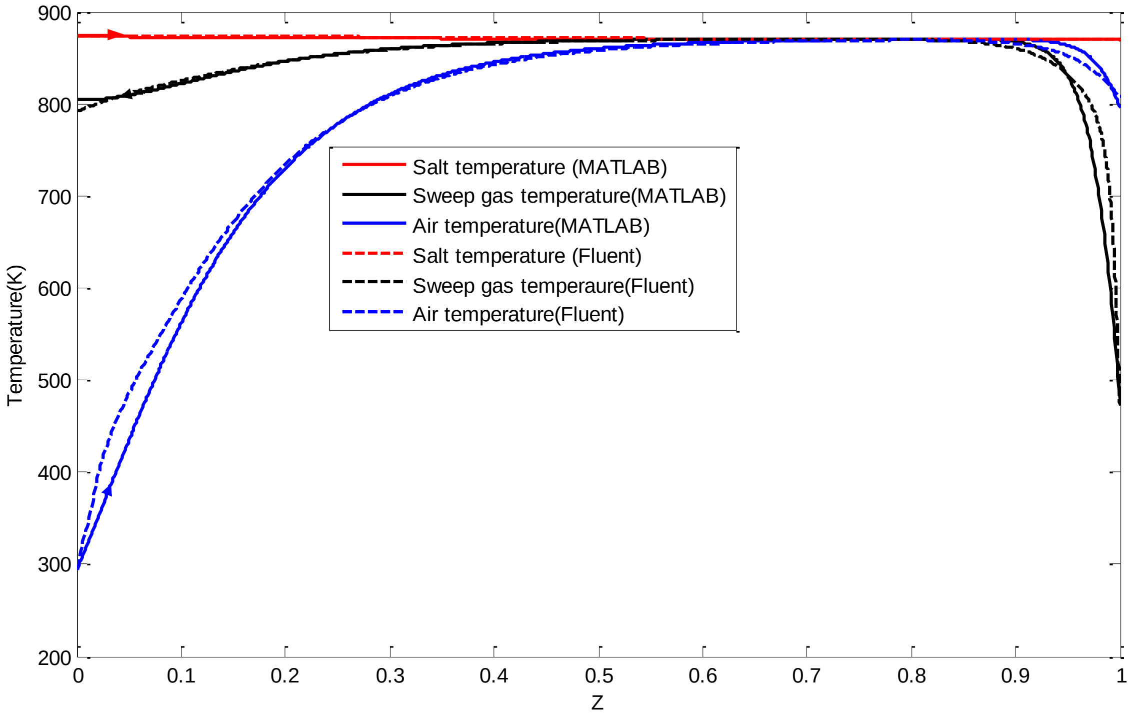

Figure 2-5. Comparison of fluid temperature profile of NDHX tube (z=0 inlet, z=1 outlet)

2.1.3 Tritium Barriers

Surface barriers are designed to have a very low diffusivity, which is ideal in preventing tritium permeation through materials. A barrier's effectiveness is characterized by its permeation reduction factor (PRF). These factors have wide ranges which depend on factors such as the type of application, content of the barrier, and the thickness of the barrier. It has also been observed that the PRF of a barrier is reduced significantly when testing was performed in a radiation field.

Table 2-2. List of candidate barrier materials for use in preventing tritium permeation [12]

Aluminides	Carbides	Oxides	Ti Ceramics
Al_2O_3	SiC	Er_2O_3	TiC
		Cr_2O_3	TiN
		SiO_2	TiO_2

Of these coatings, it appears that aluminides have the highest potential PRF with reports of over 1000. These aluminides have been observed to also have self-healing capabilities. Assuming damage to the barrier does not penetrate to the base material, it is possible for the exposed aluminide to become oxidized thus reforming the barrier. In terms of PRF, Ti ceramics appear to have the next highest performance.

Permeation barriers prevent tritium from diffusing past them. Many of these barriers are not stable in FLiBe. This requires the barriers to be placed on the non-salt side of the heat exchanger. With this placement, tritium may be allowed to permeate out of FLiBe and into the heat exchanger. The barriers will force the tritium to build up within the walls of the heat exchanger. Once the walls reach saturation, tritium will begin to permeate through the barriers no matter how high of a PRF they have.

There is other work being done to examine the effectiveness of certain finishes in reducing the amount of tritium that is adsorbed and absorbed. Mechanical and electro-polishing techniques were performed on SS316 to investigate the absorption of tritium onto the surface of the sample. The amount of tritium absorbed and adsorbed on stainless steel 316 was reduced by as much as 80% based on the polish [29].

2.1.4 **Permeators**

The overall strategy for tritium control in the FHR with permeators is shown in Figure 2-6. Redox control ensures the predominant chemical form of the tritium generated is T_2, not TF. In the tritium removal facility, the purging gas extracts and carries away T_2. The purging gas, which is inert, will go through a separate clean-up system, where tritium is finally collected. To further prevent tritium leakage, the intermediate heat exchanger is equipped with tritium permeation barriers.

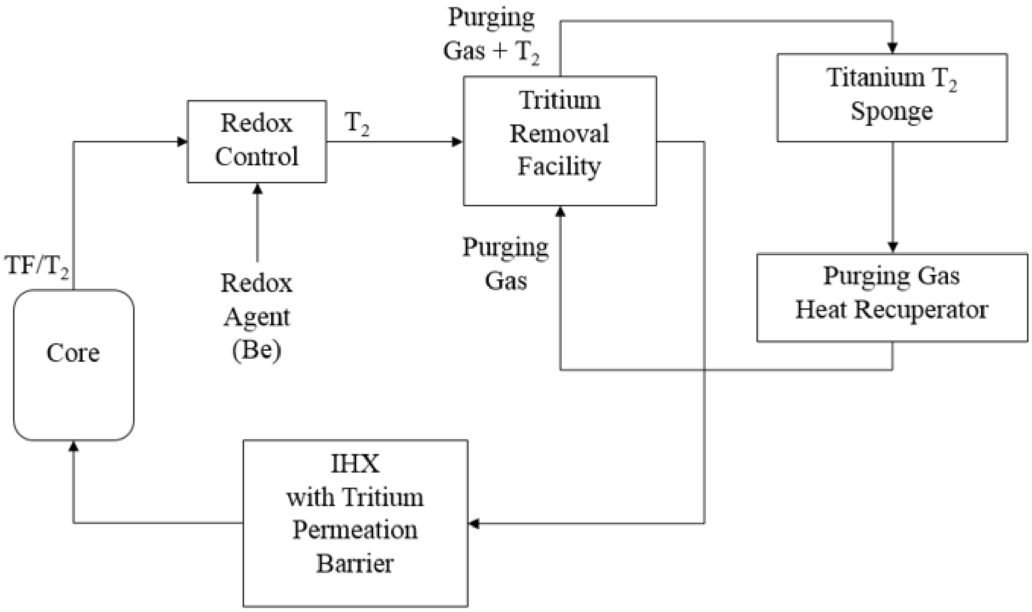

Figure 2-6. Overall FHR tritium control strategy via permeators

The working principle of tritium removal by permeators is mass transport driven by partial pressure differences. At OSU, a tritium removal facility is being designed using this principle. The facility resembles a cross-flow heat exchanger in geometry, shown in Figure 2-7. In this drawing, only a quarter of the whole tube bank is presented in the front right corner, while in the real facility, the tube bank would occupy the entire space of the facility. Molten salt flows across the tube bank, while the purging gas flows through the tubes. Tritium diffuses through the tube walls and into the purging gas. It is designed with a modular concept in mind, to meet the different demands of FHRs with different power levels. Multiple modules can be bolted together in a row, increasing the total active length of the tritium removal area, or they can be bolted side-by-side to a main pipe, splitting the molten salt flow; see Figure 2-8.

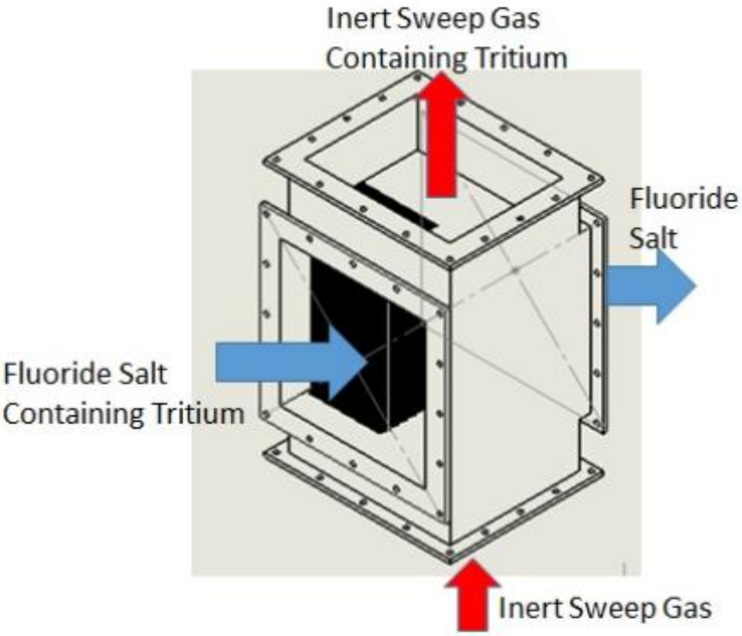

Figure 2-7. Drawing of proposed tritium removal facility

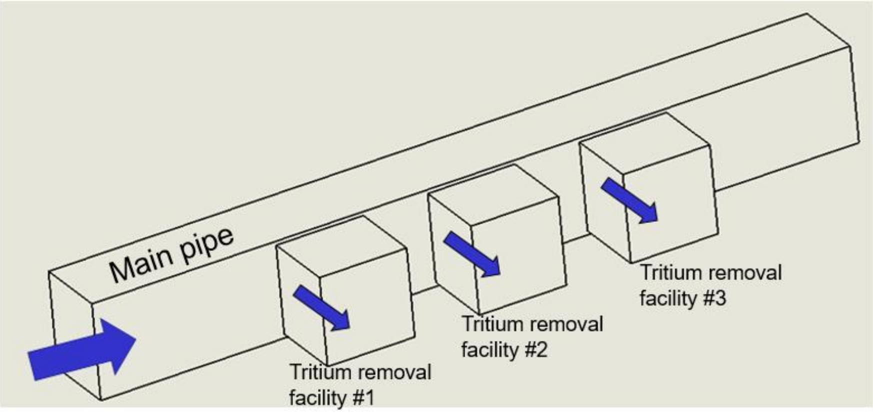

Figure 2-8. Tritium removal modular facilities connected to a main pipe

2.2 Experimental Benchmarking

Currently experimental benchmarking is undeveloped and not standardized. This will change once the technology matures, but right now the community is still learning or relearning the experimental techniques and understanding the data that the experiments are producing. A significant amount of freedom therefore exists in how we move forward and tailor our next generation of experiments. But, when doing so, it is important to be able to obtain results and data that can be directly and unambiguously comparable between experiments and institutions.

2.2.1 Common Metrics for Comparison of Experimental Results

2.2.1.1 Gas Sparging

For sparging mass transfer experiments, one figure of merit that would be constant between all experiments would be mass or volume of sparging gas used for a given dissolved gas reduction. This is possibly the best benchmark of efficiency of sparging and can be turned into an input into the TRIDENT code. The other metrics and factors that affect sparging efficiency should also be used in addition to the sparging gas volume/mass benchmark to ensure that this does ensure a legitimate comparison between experiments. These factors should be common to most or all mass transfer experiments. These factors would include liquid flow, gas flow, hydraulic fluid properties, dissolved gas concentrations, average bubble size, and key non-dimensional numbers (Re, Sc, Sh, and We).

Table 2-3. Gas sparging experiments and metrics

Experiments	Performance metrics	Experimentally measured parameters	Design parameters	Fluids used
UNM Ultrasonic enhanced sparging [30]	Time and mass of sparging gas used for DO reduction	DO Temperature	Re, Sc, Sh, We	Water/Glycerol Argon
SINAP Air Core Separator [31]	Liquid Entrainment Ratio	Pressure Flow rate Average bubble size	Re, Sc, Sh	Water Air/gas
Akita and Yoshida (1974) [32]	Bubble Swarm Mass Transfer and Holdup	Flow Rate Number of Bubbles	Re, Sc, Sh, Bo	Water Water/Glycol Water/Glycerol Water/Sodium Sulfide Air/Oxygen

Gas–liquid mass transfer in a novel forced circulation loop reactor [33]	Mass transfer coefficient and mass transfer efficiency	Hold up Flow Rate DO	k_La (volumetric mass transfer coefficient)	Water/Oxygen

2.2.1.2 Tritium Getters

Tritium experiments using getters as absorption mechanisms can be benchmarked by measuring the amount of tritium which is absorbed on the getter. For metal hydrides, this process is easily achieved as hydrides are able to release the tritium they have absorbed which makes them ideal systems for temporary storage applications.

2.2.1.3 Double-Wall Heat Exchangers

Double-wall heat exchangers are being proposed for a variety of locations within the FHR system such as the intermediate heat exchanger (IHX) and the DRACS heat exchanger (DHX). Therefore, initial studies are aimed to determine the heat transfer performance and for code benchmarking. Future studies could then be focused on determining viable tritium permeation performance. Figure 2-9 explains current experiments and their focus on heat transfer for double wall systems.

In a double-wall heat exchanger tritium may permeate from the shell-side fluid into the secondary or tube-side fluid. The double-wall tube provides the unique ability to fill the intermediate annulus with a system to prevent the tritium from permeating through it. This system can use a gap fluid or sweep gas to sweep the tritium out of the heat exchanger as it enters the intermediate annulus. Other systems could include coatings or barriers, which prevent tritium from permeating, and getters which would fill the intermediate annulus and absorb tritium. The performance of a barrier or any system which can be implemented within a double wall heat exchanger can be can be measured by examining the tritium concentrations in the primary stream and the resultant concentration in the secondary fluid stream. The goal of any tritium removal system relevant to a double-wall heat exchanger should be to reduce the amount of tritium which passes from the primary fluid into the secondary fluid. Therefore, viable metrics for any system should be able to compare the reduction in tritium concentration in the secondary fluid.

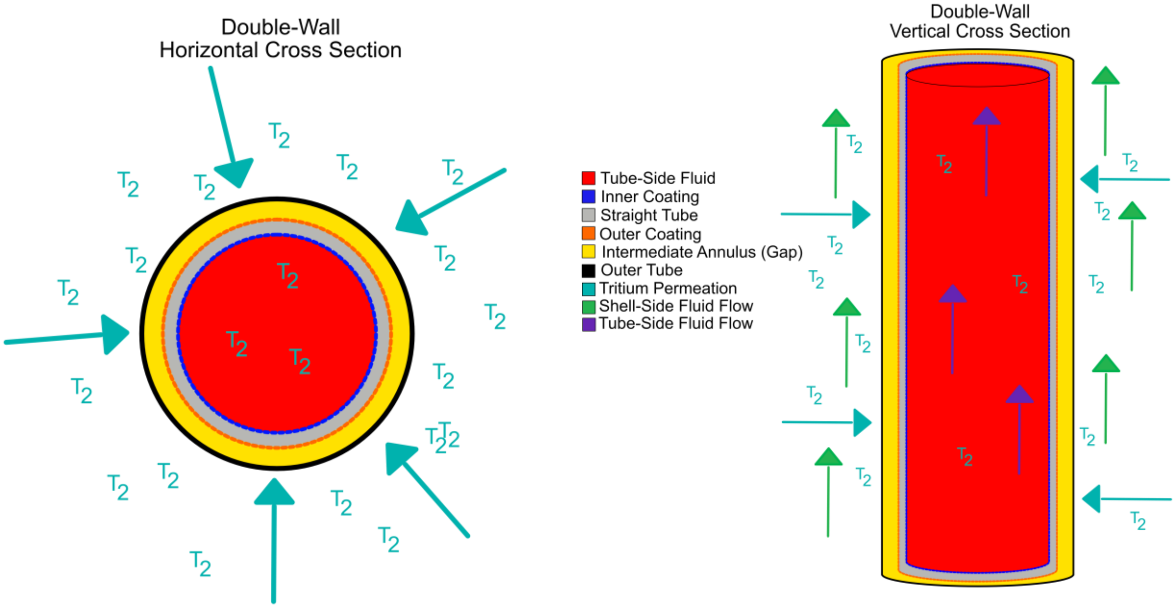

Figure 2-9. Horizontal and vertical cross sections of a double wall tube describe tritium permeation from the shell side fluid to the secondary fluid through the walls and intermediate annulus of the tube

Table 2-4. Double-Wall Heat Exchangers

Experiments	Performance metrics	Experimentally measured parameters	Design parameters	Fluids used
UNM Double-Wall Twisted-Tube IHX	Overall Heat Transfer Coefficient, Heat Transfer Rate, Pressure Drop	Absolute Temperature Difference, Mass Flow Rate	Re, Pr, Nu, Gr	Water, Dowtherm A, S-CO2, possibly Helium, Argon or Nitrogen
OSU Natural Draft	Heat Transfer Rate	Temperature, Mass Flow Rate	Re, Pr, Nu, Gr	FLiNaK, Ar or He

2.2.1.4 Tritium Barriers

As stated earlier, common benchmarks for permeation barriers refer to the permeation reduction factor (PRF). The PRF is a comparison of the reduction in tritium that has permeated through a metal with and without a barrier. The PRF and ultimately barrier effectiveness is dependent on multiple other characteristics of the system such as the base metal it is applied to, application process and the partial pressure of tritium in the primary fluid.

2.2.1.5 Permeators

To test the effectiveness of the designed tritium removal facility, a scaled down experiment has been designed. The schematic of the experimental loop is shown in Figure 2-9. FLiNaK is pumped through a loop, which consists of a H_2 dissolution station and a small-scale removal facility. A 5-by-5 tube bank is used in the small scale tritium removal facility designed for the validation experiment. The H_2 carried out by the purging gas from the removal facility is quantitatively analyzed by a hydrogen sensor. At equilibrium conditions, the amount of H_2 dissolving into FLiNaK is the initial H_2 concentration at the molten salt inlet of the removal facility. By recording the H_2 flow rate in the outlet purging gas at steady state, the overall mass transfer coefficient of the experimental facility can be calculated. The results can be used to determine the effectiveness and efficiency of the proposed tritium removal facility design. Additionally, it is hoped that the results can be scaled up to obtain the removal effectiveness for the full-scale tritium removal facility.

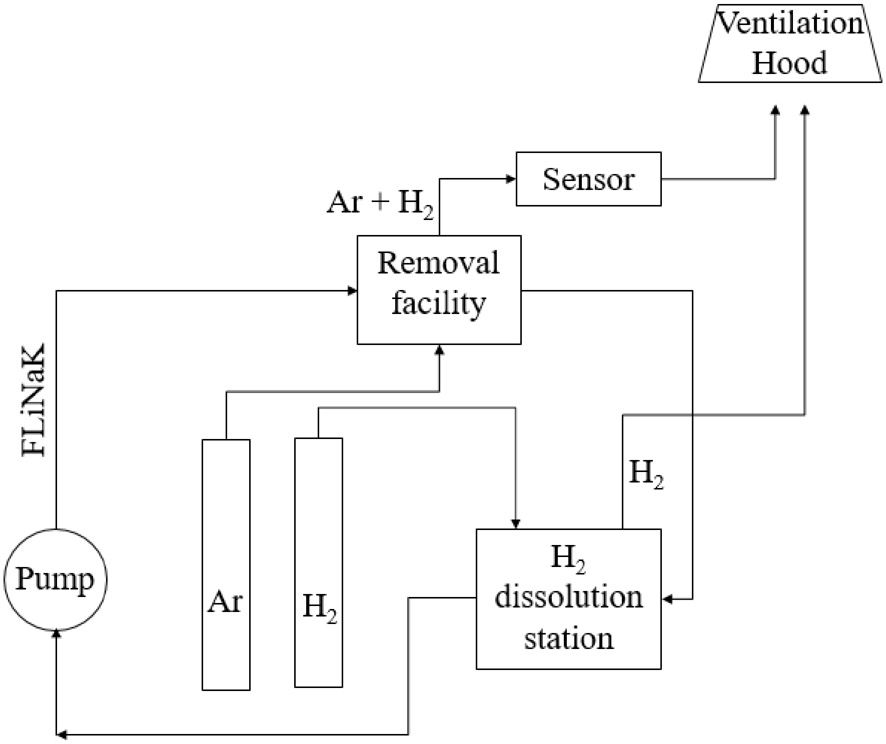

Figure 2-10. Schematic of the permeator removal facility validation experiment

As shown in Figure 2-10, the experiment consists of a molten FLiNaK loop, a H_2 loop, and an Ar purging gas loop. Molten salt is driven through the loop by a pump. It picks up H_2 at the H_2 dissolution station, and flows across the tube bank in the removal facility. Part of the H_2 dissolved in the FLiNaK is removed in the removal facility. Ar is used as the purging gas in this experiment. It flows through the tube bank of the removal facility and carries away the H_2 transporting out of the FLiNaK. The outlet Ar with H_2 will go through a hydrogen sensor, where the concentration of H_2 is measured and recorded. The mixed gas is then vented out through a ventilation hood.

2.2.2 **Hydrogen and Deuterium Surrogates for Tritium**

Hydrogen has been the default surrogate for tritium for good reason. It is nearly identical in all respects, except for mass. But, as we move forward in using hydrogen as a surrogate, the question that comes up is how exactly hydrogen and tritium differ in behavior. The characterstics of interest for FHR application are solubilities, diffusivities, kinetics, and thermodynamics.

The diffusivity of a gas in metal is generally described by an Arrhenius relation and classical diffusion theory states this relation shown in equation (2-1), where D is the diffusivity and m is mass of hydrogen and tritium.

$$\frac{D_T}{D_H} = \sqrt{\frac{m_H}{m_T}} \tag{2-1}$$

This has been shown to be a good approximation for temperatures above ambient and for face-centered cubic (FCC) metals [34].

Studies have been performed to experimentally determine the transport properties of hydrogen isotopes in various media of interest, such as palladium, 316L stainless steel, or tungsten.

Reiter et al. performed a study to measure the solubility, diffusivity, and permeability of hydrogen and deuterium in 316L stainless steel. Stainless steel cylinders were loaded with either of the isotopes under pressure and then placed in an evacuated chamber. The pressure increase in the chamber from the resulting desorption process was measured and used to calculate these parameters; see Figure 2-11. A set of equations were then used to calculate them for tritium under common assumptions [35].

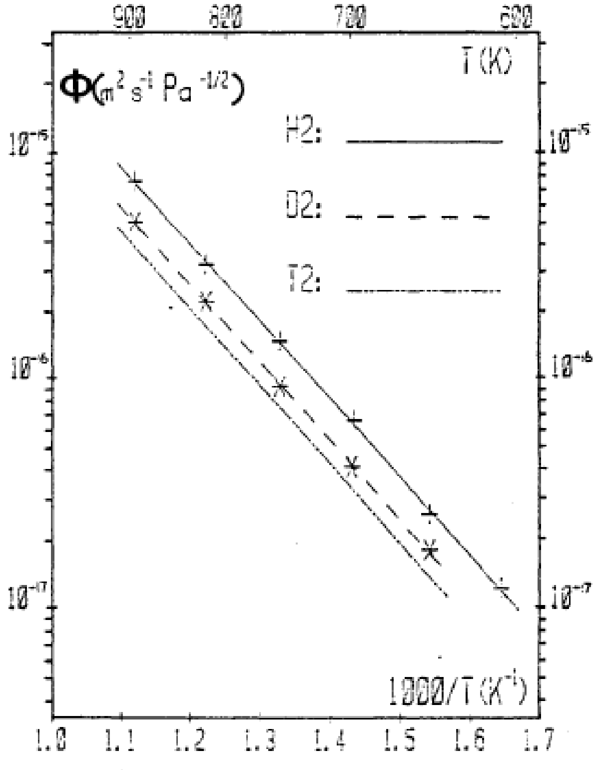

Figure 2-11. Permeability of hydrogen, deuterium, and tritium gas through 316L SS [35]

Lee et al. performed another isotopic study of hydrogen permeability in stainless steel 316 (316L SS) was performed. Gas was forced through a metal membrane via a pressure difference, and the permeation was measured. The permeability, diffusivity, and solubility Arrhenius relations were obtained for both hydrogen and deuterium gas with respect to 316L SS [36]; see Figure 2-12.

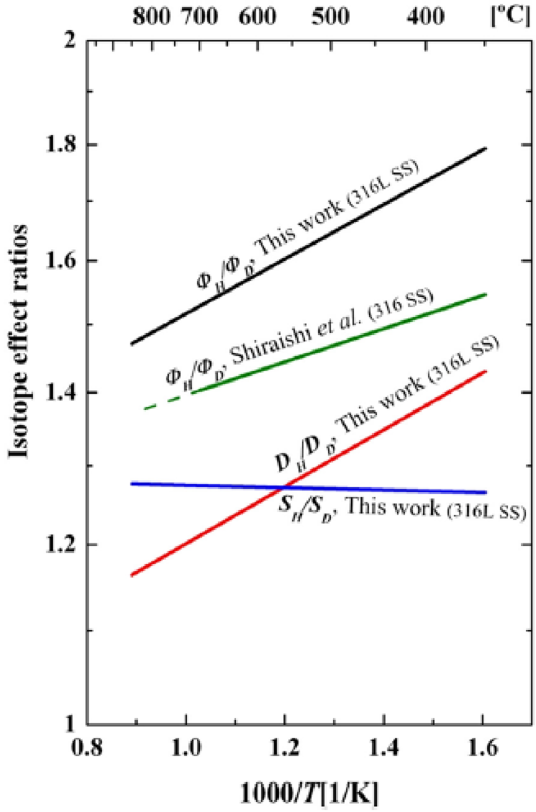

Figure 2-12. Ratios of respective permeability, diffusivity, and solubility of hydrogen to deuterium in 316L SS [36]

To a first approximation, the use of hydrogen as a surrogate is useful. But, if hydrogen is used in lieu of tritium, there will be some slight aberration between the experimental results obtained with hydrogen versus tritium. Because using a surrogate is an approximation, it would be best to use both hydrogen and tritium to verify that the approximation is acceptable as well as quantify the differences between hydrogen and tritium.

2.3 Conclusions

It is most likely that multiple methods will be implemented to address the tritium challenge in the final design of an FHR. The separation techniques surveyed in this section were gas sparging, double-wall heat exchangers, tritium barriers and use of permeators. A key conclusion from the workshop discussion is that common metrics need to be identified for each method, so that comparisons can be made across research groups, and eventually also among the different separation options. Subsequently, as better characterization becomes available for each of these separation methods, it will be possible to define experimental and modeling benchmarks for each of the methods; at the present moment, definition of benchmarks is most likely premature.

3 Graphite and other carbon forms

3.1 Role of Graphite and Carbon in the FHR

The FHR fuel (TRISO) contains silicon carbide coating and pyrolytic carbon that serve as the neutron moderator. Thousands of TRISO fuel particles are encapsulated in graphite matrix to form a fuel pebble with 3 cm diameter. Carbon/graphite traps tritium. In the MSRE, it was discovered that about 15% of the tritium that was generated was trapped in the graphite moderator. Tritium holdup in the carbon may be significant, although there are order-of-magnitude uncertainties for maximum hydrogen solubility in graphite at high temperatures. If all tritium were absorbed in the fuel elements in a pebble-bed FHR, a loading of 2-10 ppm by weight tritium to carbon ratio (wt% T/C) would result. In a pebble bed reactor, the pebble fuel is circulated through the reactor core with a residence time of approximately one month with a typical pebble circulating through the core 10 to 15 times before being discharged as spent nuclear fuel. If the tritium in the pebbles was removed before returning to the reactor core by heating, the carbon in the core could be used to remove tritium from the salt.

In FHR, it is convenient if the fuel elements are efficient sinks for tritium but there are also concerns. In an over-temperature transient the tritium may be released quickly. In FHRs much of the carbon remains in the core for years and the carbon would saturate with tritium. The equilibrium quantities of tritium in the core depend upon the average tritium levels in the coolant; thus, inventories can be minimized by maintaining low levels of tritium in the coolant. This has a practical implication for reactor systems with carbon in the core. If an external-to-the core tritium removal system can maintain low tritium levels in the salt, short-term outages of that system are acceptable because the carbon in the core will collect the tritium.

Recent developments may enable small carbon beds to efficiently remove tritium from liquid salts. There are two considerations (1) surface area of carbon and (2) ability of carbon to adsorb tritium.

Surface area. For tritium to be removed from liquid salt, it must be transported to a surface be it the liquid-gas surface of a sparger, the metal surface of a permeator or a carbon surface. The more surface area, the faster is the potential ability to remove tritium. The total specific surface area (due to the large porosity in carbon microstructure) of many carbon materials are large relative to other materials—the basis for using carbon as a substrate in many catalysts that are then coated onto the carbon.

Tritium removal. The second requirement for tritium removal is capture of the tritium once it reaches the liquid-carbon interface. Outside the reactor core there is no need for nuclear grade graphite. The processing of carbon to produce graphite with dimensional stability under high neutron radiation alters its sorption capabilities. Without the requirement to withstand high neutron fluxes, an out-of-core carbon bed can select carbons to maximize tritium removal—potentially with orders of magnitude better performance. Figure 4.1 shows recent experiments for hydrogen sorption with a nuclear (ISO-88) and non-nuclear grade graphite with several orders of magnitude better performance with some of the new carbon forms. There is the potential that a small carbon bed would efficiently remove tritium from the salt—similar in design to an ion exchange bed in a light water reactor.

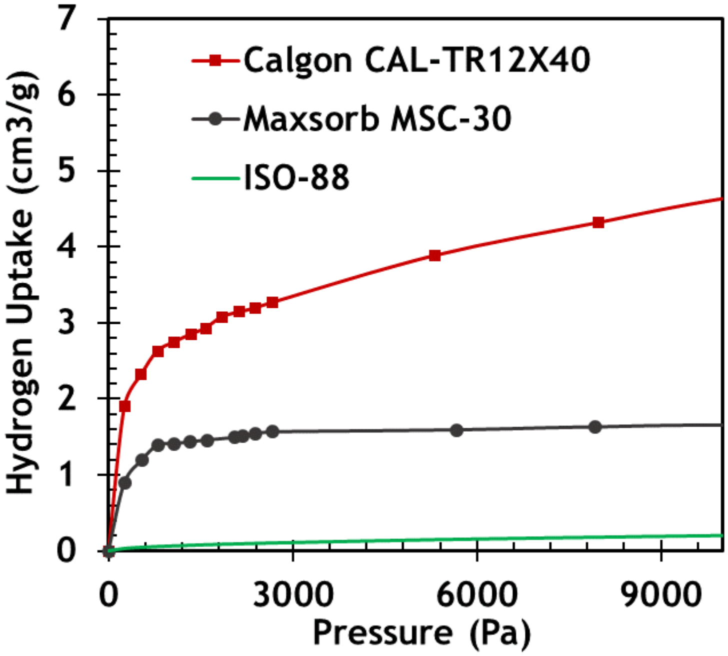

Figure 3-1. Hydrogen Adsorption on Different Carbon Forms at 700^{o}C

These recent developments are a consequence of efforts to develop carbon forms for (1) hydrogenation catalysts for the chemical industry, (2) hydrogen storage and (3) carbon electrodes for fuel cells. This has resulted in major improvements in understanding hydrogen carbon systems and thus creating new tritium control options.

The implications of this work is that the behavior of tritium and carbon is required to understand (1) tritium inventories in the reactor core associated with the fuel and moderator and (2) carbon as a tritium removal system. These are different carbon forms designed for different purposes and thus multiple carbon forms must be characterized.

3.2 Graphite Characterization

Microstructure of graphite differs from type to type due to raw material, particle size of powder, shape forming method, graphitization temperature and other factors. Parameters of graphite microstructure include density, open and closed porosity, pore size distribution, interplanar size, lattice parameter, and anisotropy of grain orientation. In FHR design, one major concern is tritium production in reactor core produced by neutron activation with molten salt (FLiBe or FLiNaK), and with large graphite cross section composed of fuel pebble, reflector, graphite pebble, it is interesting to know the ability of graphite for tritium absorption. Literature shows tritium absorption in graphite will be greatly affected by particle/grain size and microstructure defects in graphite due to incomplete graphitization or radiation. Both MIT and UW Madison are working on graphite characterization to understand what properties control tritium uptake; MIT works with different types of graphite and carbon materials while UW Madison focuses on nuclear grade graphites (IG-110 and graphite matrix A3). This section presents some of the work at both MIT and UW Madison.

The graphite/carbon material MIT will characterize is listed below. The characterization techniques are shown in Table 3-1.

- Graphite: IG-110U, A3-3
- Irradiated Graphite: IG-110U, A3-3
- Activated Carbons: Maxsorb MSP-30, Calgon CALTR12x40, Cabot Norit PAC200
- Graphene Nano-platelets Nannoinova GraphenitOX

Table 3-1. Methodology of Graphite Microstructure Study in MIT

Parameter	Technique	Instrument	Data Analysis	Note
Surface Area/ Total Pore Volume	Brunauer-Emmett-Teller (BET)	QuantaChrome IQ-C		Using N2 at 77K
Pore Size Distribution	QSDFT⁽¹⁾/NLDFT⁽²⁾	~	ASiQWin 4.01	Pore size from 2-50nm
Micro-Scale Porosity	Imaging Processing Toolbox	~	MatLab	> 1µm [37]
Lattice Parameter - L_a and L_c	X-ray powder diffraction	~	PANalytical HighScore Plus	

(1) QSDFT – Quenched Surface Density Functional Theory [38]

(2) NLDFT – Non-linear Density Function Theory [39]

UW Madison is mainly working on two types of nuclear grade graphite: IG-110 and matrix graphite A3. Table 3-2 summarizes the differences of IG-110 and A3 from raw material and manufacturing process.

Table 3-2. Comparison between IG-110 and A3

Item	A3	IG-110
Raw Material	Natural Graphite-64 wt%, Synthetic Graphite-16wt%,High purity novolac resin-20wt%	Petroleum Coke/Coal tar Pitch
Manufacturer	ORNL	Toyo Tanso Co. Japan
Formation	Promess Press @ 1mm/s	Cold Isostatic Pressing
Heat Treatment Temperature	650 °C	~2100°C
Grain Size	unknown	20µm

Initial graphite characterizations have been done is porosity and pore distribution by density measurement kit, BET and Mercury Porosimetry, SEM and Optical Spectroscopy, X-ray Diffraction and Raman. Detailed technique information and preliminary comparison results are shown in Table 3-3 and Table 3-4.

Table 3-3. Summary of techniques for graphite characterization in UW Madison

Parameter	Method	Technique
Porosity	Archimedean Immersion	Simple Density Measurement Kit
	BET	Quantachrome® ASiQwin™
	Mercury Porosimetry	QuantaChrome Poremaster
	MatLab	Imaging Processing Toolbox
Lattice Parameter	Bragg's law	X-ray Diffraction
	$L_a=2.4*10^{-10}\lambda_{laser}^{4}(I_D/I_G)^{-1}$	Raman
Graphitization	$(d_{002}^{g=0}-d_{002})/(d_{002}^{g=0}-d_{002}^{g=1})$	X-ray Diffraction
Crystallite Size	Scherrer equations(1)	X-ray Diffraction

(1) Scherrer equations: $L_c= 0.91\lambda/\beta\cos(\theta)$, using 002 peak; $L_{\perp}= 1.84\lambda/\beta\cos(\theta)$, using 101/112 peak

Table 3-4. Microstructure parameters for A3 and IG-110

Measurement	A3	IG-110
Open Porosity (%)	*TBC*	*TBC*
Close Porosity (%)	*TBC*	*TBC*
Average Pore Size (μm)	2.720	0.8104
Specific Surface Area (m^2/g)	2.564	1.018
Lattice Parameter (nm) - a	0.24657	0.24626
Lattice Parameter (nm) – d_{002}	0.33645	0.3374
Crystallite Size (nm) - L_a	27.84	21.25
Crystallite Size (nm) – L_c	35.28	27.21
Graphitization	91.86	82.56

The following figures, Figure 3-2 through Figure 3-5, show porosity related analysis for both A3 and IG-110, including pore size, pore size distribution, specific surface area by BET, mercury porosimetry and image processing using the MatLab image processing toolbox. All three methods give different pore size range: BET shows both graphites with pore size peaks at around few nm; mercury porosimetry shows peaks around µm level; the imaging processing from MatLab gives pore size distribution also in the nm range. Mercury porosimetry and Matlab porosity analysis show consistent comparison results for IG-110 and A3, IG-110 showing pore size in both large and small scale range, while A3 showing pore size only in the small scale range, see Figure 3-3 and Figure 3-4.

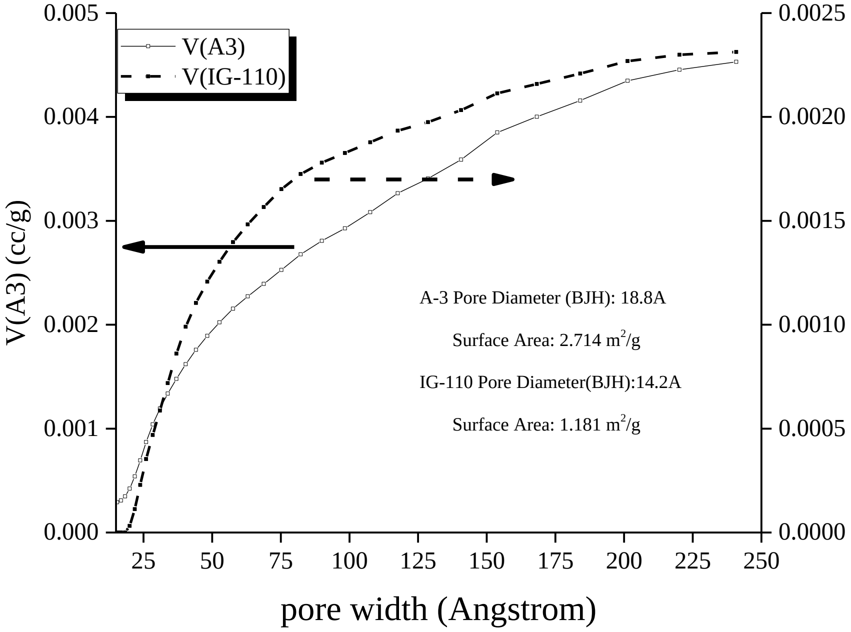

Figure 3-2. Pore dimension of A3 and IG-110 calculated from BET analysis

The gradient of the curve indicates the pore width for A3 and IG-110. The calculated pore diameter and surface area are shown in the text, showing A3 has larger pores as well as larger specific surface area compared to IG-110.

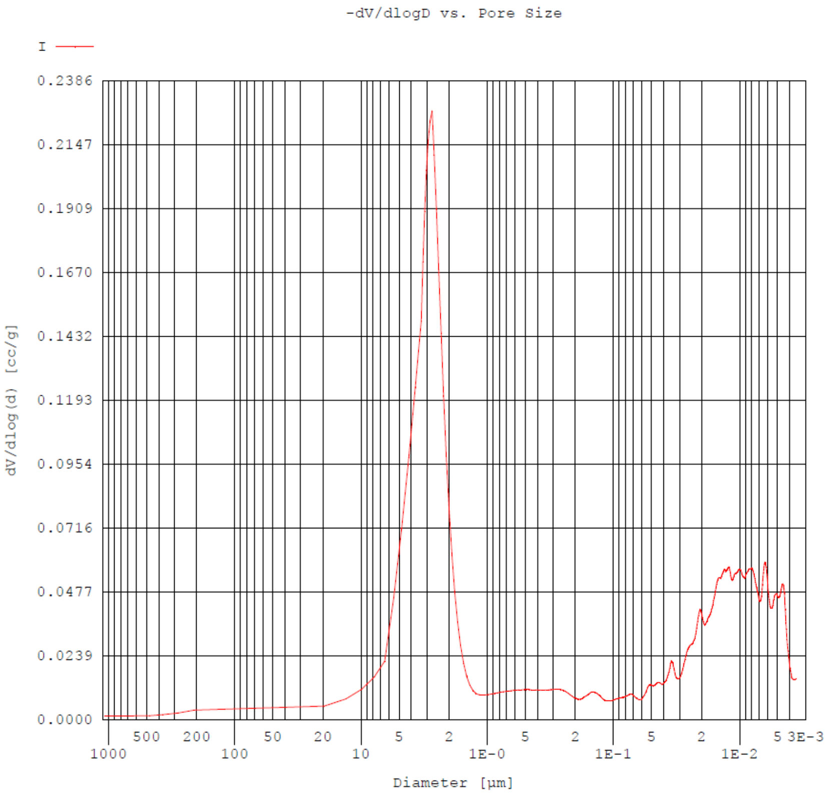

Figure 3-3. Pore Distribution of IG-110 from Mercury Porosimetry. IG-110 shows intense peak at pore diameter around 2-9 µm and minor peak at around 5-20 nm.

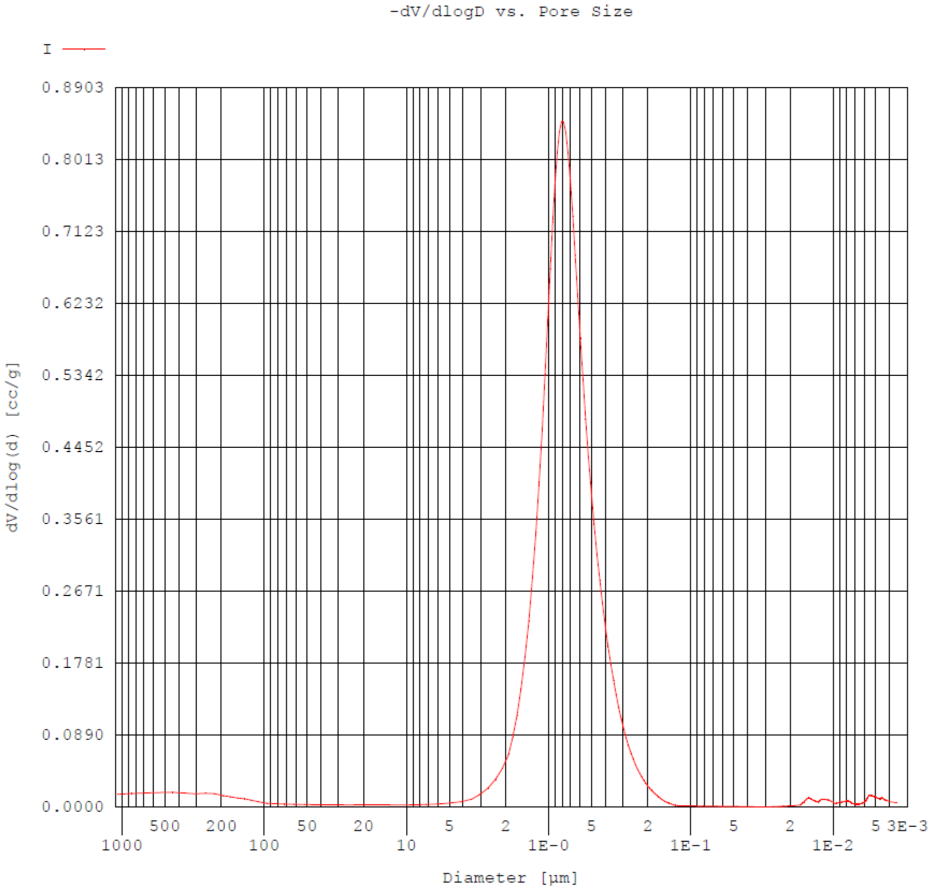

Figure 3-4. Pore diameter of Matrix A3 from mercury porosimetry. Matrix A3 shows intense peak at pore diameter around 0.2-2 µm and almost no pores in the nm range.

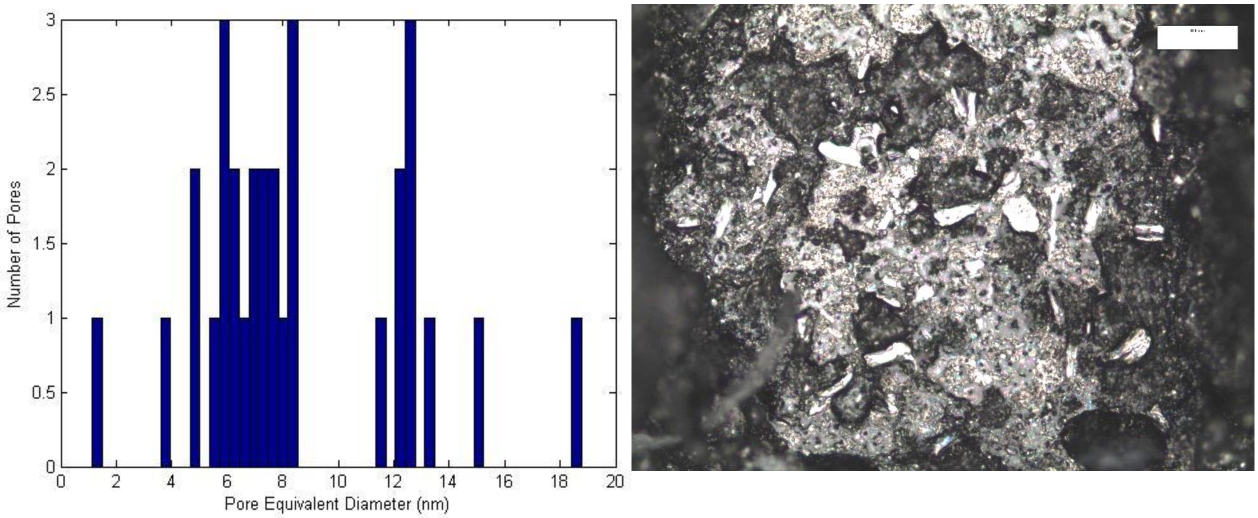

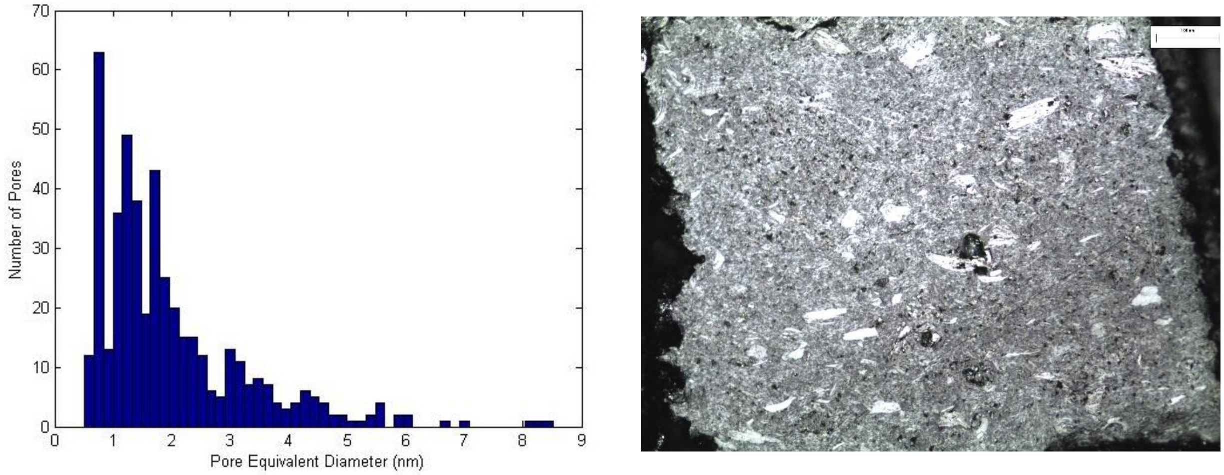

Figure 3-5. A3 pore diameter distribution (top left) by MatLab imaging process toolbox with image from optical microscopy (top right). IG-110 pore diameter distribution (bottom left) with image from optical microscopy (bottom right). Top left plot indicates that pore diameter in IG-110 falls into two regions and bottom left plot shows that the pore diameter in A3 concentrates in one region.

3.3 Salt-Graphite Interaction

Tritium transport from salt to graphite depends upon the salt-graphite interface. Higher surface area implies higher rates of mass transfer from salt to carbon. To understand the kinetics of salt-carbon tritium transport, the surface interface must be understood.

The experimental setup is shown in Figure 3-6. Shaft 1 is top of the central rod with small diameter and a orfice at the bottom to release over pressure in the crucible due to temperature increase. Shaft 2 is the bottom region with larger diameter and two through-all holes holding up sample rod. Square graphite samples of 1mm thickness are hanged on both ends of thin sample holder rods. The holders are used to prevent the light graphite sample from float in the molten salt, and to support the weight of the samples before they are immersed in the salt. The crucible and sample holders are made of high purity graphite to prevent introduction of metallic impurities or metal alloy corrosion products in the salt.

The whole experimental apparatus sits inside a vertical furnace that can operate up to 1200 ^{o}C. The experiment is performed inside a glove box with Argon atmosphere, with O_2 < 1ppm and H_2O < 1 ppm. The required components for the experiment are shown in Table 3-5. In the figure, it shows the graphite crucible, customized central rod and thin sample-holder rods.

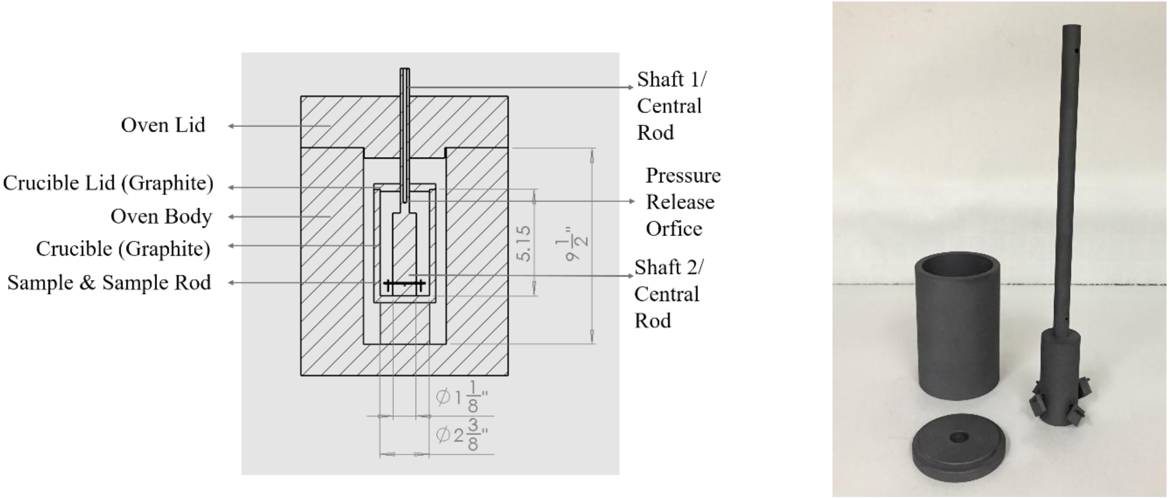

Figure 3-6. Experimental setup for salt intrusion experiment

Table 3-5. Sample description prepared for FLiBe intrusion experiment

Sample ID	**Material**	**Weight (g)**	**Surface Area (mm^2)**	**Dimension (mm)**
FIE-009	IG-110	0.46640±0.00003	311.788	10.6*10.69*2
FIE-010	IG-110	0.61898±0.00003	333.0302	9.78*9.37*3.91
FIE-007	A-3	0.52002±0.00008	384.869	10.97*11.01*3.26
FIE-006	A-3	1.06414±0.00002	544.8504	10.95*10.98*6.94

SEM/EDS, XPS, GDMS or other elemental analysis will be done on the immersed samples. The following figures show initial result we get from SEM/EDS. From the image, we can clearly see salt particles from the size nanometer level to micrometer level and next step will be finding the way to quantify salt quantity and study the salt depth profile into graphite sample.

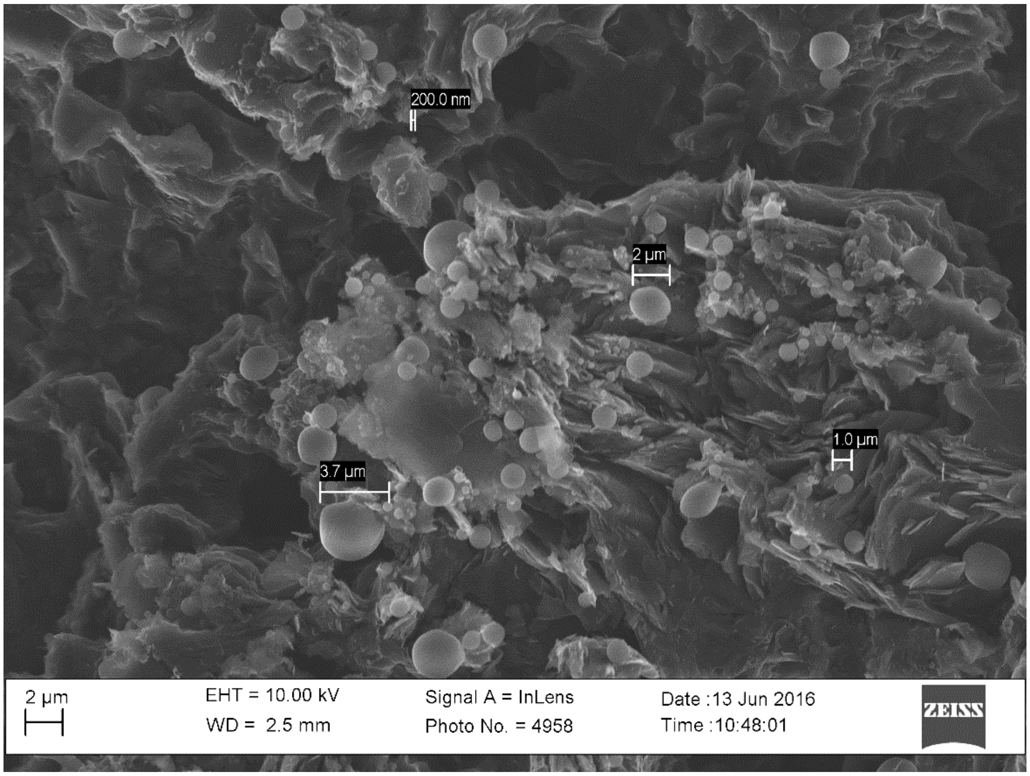

Figure 3-7. Image of graphite sample which is immersed into salt under 650 C for 12hr (from SEM)

The Be and Li are too light for the EDS detector to be able to pick up any signal from these elements, but it can pick up F signals. Figure 3-8 clearly shows F peak is the main peak at point 1 in the above image, so we think the particles shown in both Figure 3-7 and Figure 3-8 are salt.

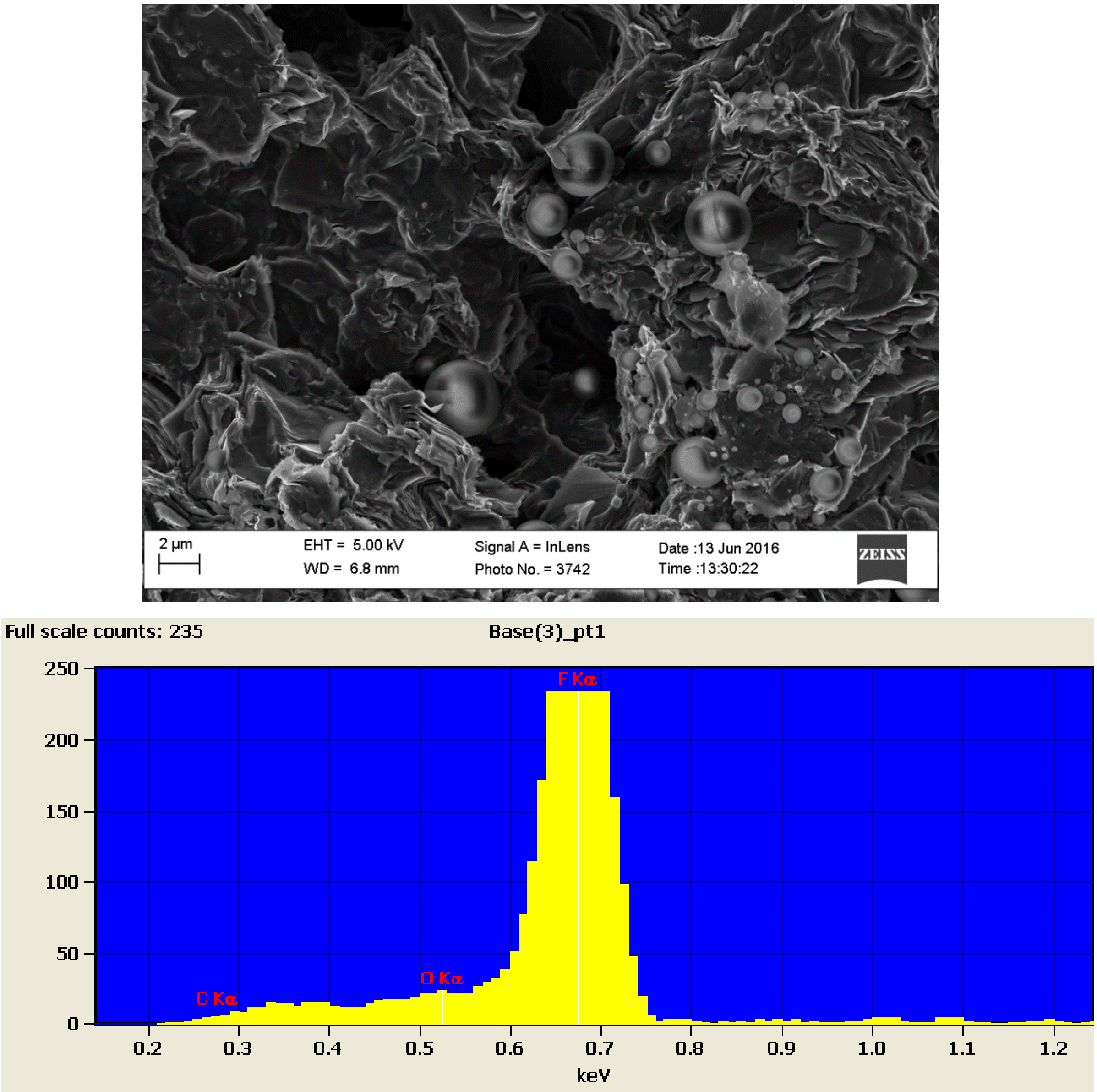

Figure 3-8. EDS analysis for FLiBe intruded IG-110 (above: SEM image, below: EDSv spectrum analysis)

3.4 Tritium in Graphite

In UW Madison, we want to build up a system using constant volume method to study tritium absorption into graphite by measuring pressure difference between sample container and a known pressure reservoir. Figure 3-9 is the experiment setup which will be build inside glovebox. By measuring the pressure difference using high sensitivity differential pressure gauge, we expect to be able to calculate tritium absorption into graphite as well as the absorption rate.

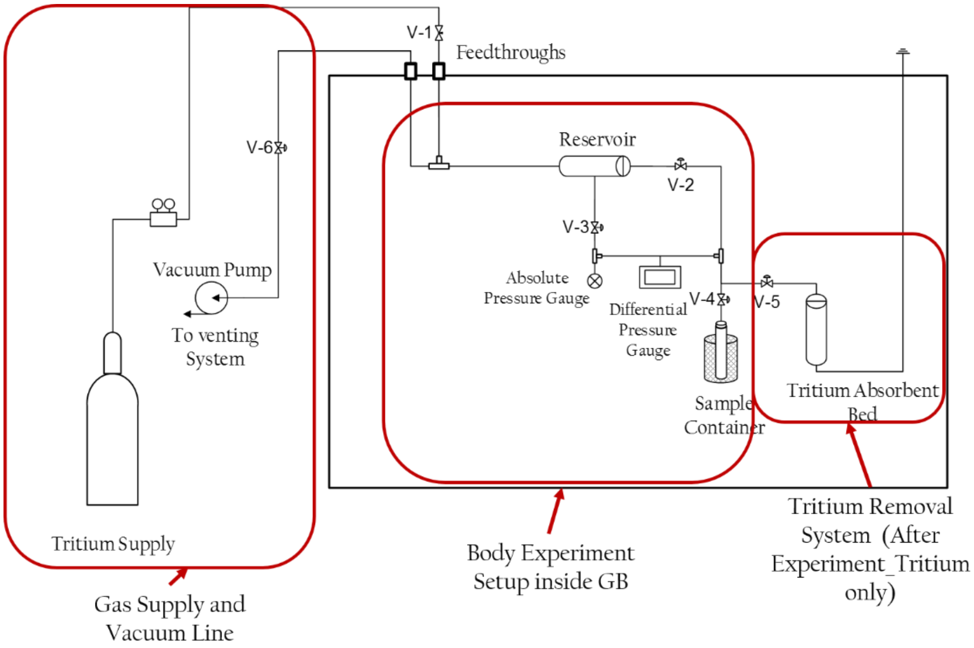

Figure 3-9. Experimental setup to study hydrogen absorption in graphite

In MIT, Tritium adsorption experiments are conducted using a QuantaChrome IQ-C and a Pfeiffer Prisma Plus Mass Spectrometer. The instrument flow diagram is shown below and is set up to measure chemisorption (chemical adsorption with activation energy).

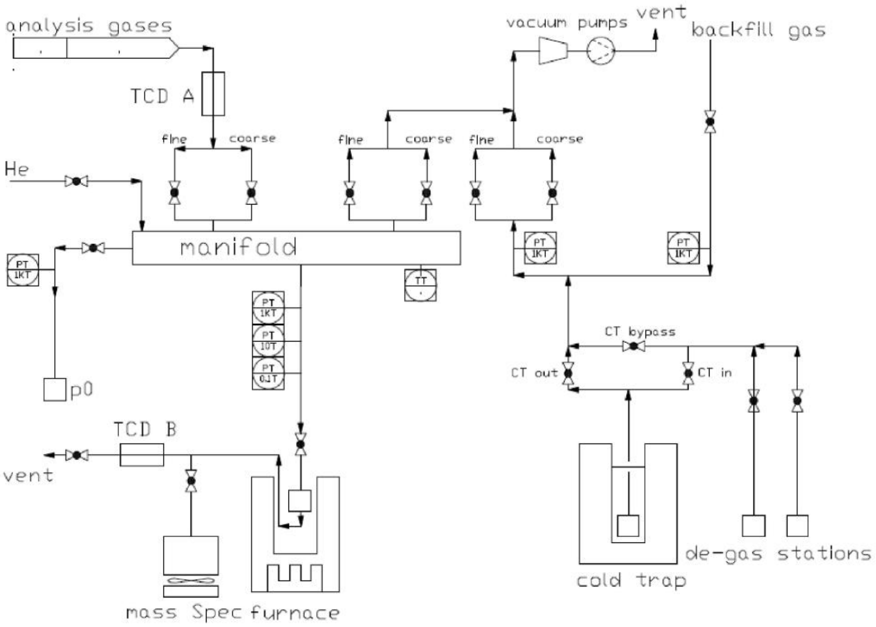

Figure 3-10. QuantaChrome IQ-C Chemisorption Analysis Flow Diagram

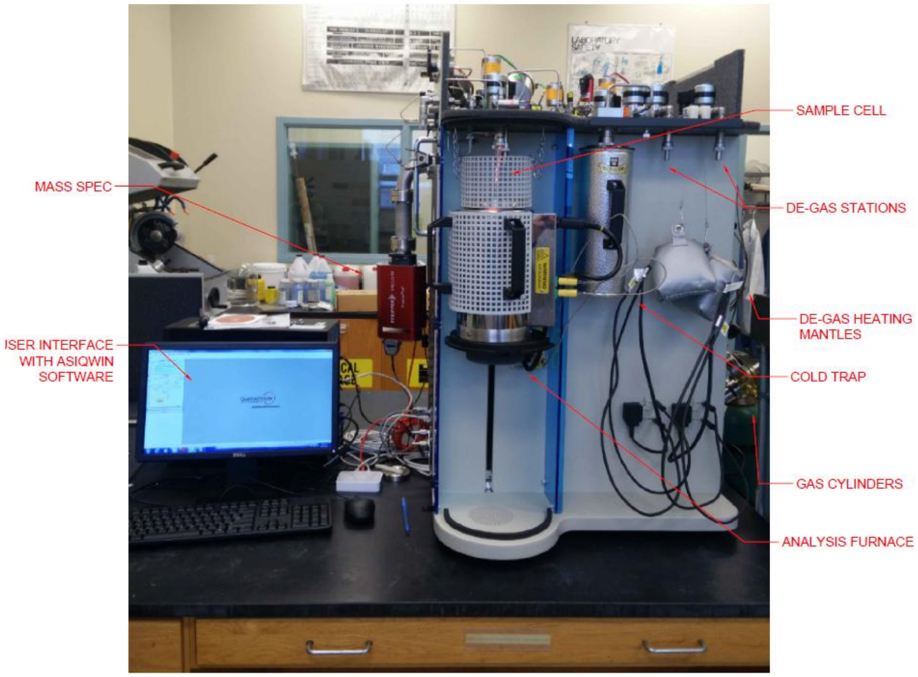

Figure 3-11. QuantaChrome IQ-C Instrument Front View

As shown in Figure 3-10, the instrument system is equipped with pressure transducers, a dosing manifold and control valves that allow precise dosage of the analysis gases into the sample. Additionally, thermal conductivity detectors and a mass spectrometer can indicate the species and quantities adsorbed and desorbed from the sample. The relevant parameters that will be measured is summarized below.

- Equilibrium Isotherms and Adsorbed Volume: Using apparatus in Figure 3-11, the manifold and sample cell are evacuated with vacuum pumps. Stepwise and at constant temperature, the adsorptive gas is dosed into the sample cell and equilibrated. Pressure transducer measurements are used to calculate the volume of adsorbed gas onto the sample. The run will be repeated for temperatures between 600-700 ^{o}C. Langmuir, Freundlich and Temkin methods can be applied to determine the relevant adsorption mechanism and solubility curves [40].
- Heat of Adsorption: Using data from equilibrium isotherms measured and the Clausius-Clapeyron equation (Ln[P] vs. 1/T), the heat of adsorption and adsorbed volume (or surface coverage) can be determined.
- Trapping Activation: Temperature programmed desorption with thermal conductivity detector (TCD) and Quandrapole Mass Spectrometer (QMS) readings at different heating rates from temperatures between 400-1100^{o}C. Application of the Kissinger equation yields the activation energy of traps [41].
- Apparent Diffusivity: Known volumes of adsorptive gas are dosed into the sample cell and the isothermal pressure variation with time is monitored. Fickian diffusion laws for known geometries can be applied to determine the diffusivity [42].

3.5 **Other Species in Carbon: Corrosion and Activation Products**

Under FHR operating temperatures 600-700^{o}C in a hydrogen atmosphere, it is possible that hydrocarbon vapors (CH_4 or C_2H_6 for instance) can form depending on the type of carbon [43,44]. Any reactant products that are created under conditions will be detected by mass spectrometry during experiment shown in Figure 3-11.

3.6 Benchmarking

3.6.1 Graphite characterization standards

One type of graphite material should be chosen between MIT and UW Madison or other universities or research institutions, we should benchmark the characterization results and to set up the standard for future research. We propose IG-110 from MIT since MIT has a stock of IG-110 with known source, and can be purchased from the market. Sample preparation procedures for different techniques are still to be discussed and determined.

3.6.2 Common stock materials

Various grades of graphite under investigation are listed below in Table 3-6. The manufacturing details are listed in Table 3-2.

Table 3-6. Type of graphite stocked at UW Madison

Graphite Type	Provider
IG-110	MIT
A3	INL/ORNL
Irradiated A3	INL

3.7 Conclusions

There are many challenges related to tritium in molten salt-graphite systems. Many factors need to be taken into consideration, including salt chemistry, effect of graphite microstructure, tritium diffusion through salt-graphite interface, and effects of other gaseous impurities or fission products. There is also research focusing on removing tritium from outside of reactor core, and this broadens the choice of carbon/graphite materials. It is important to correlate the research of graphite microstructure analysis with that of hydrogen diffusion in graphite/carbon materials and graphite-salt system to better understand what is controlling hydrogen transportation in FHR system. Collaboration is required for performing this research due to its complexity, and it involves interdisciplinary effort.

4 Salt Chemistry

This section presents the on-going research work in both University of Wisconsin - Madison and Ohio State University related to salt chemistry. The current status of electrochemistry techniques used to study corrosion, fluoro-acidity of salts and tritium transport is discussed in this part. This section also presents the motivation for development of spectroscopy techniques in molten salts and the reports methods used to safely work with beryllium-containing salts.

4.1 Electrochemistry

4.1.1 Dynamic Probe Measurements

The redox potential of the salt determines the relative concentrations of H_2 and HF in the salt. Knowing redox potential is required to understand experiments. In a power reactor, a method to measure redox potential will be required to control the salt redox potential by the appropriate addition of redox agents.

The Sridharan group at UW Madison has developed and built a dynamic reference electrode probe for the purpose of measuring the chemical potential of prepared FLiBe batches and the change in chemical potential upon exposure to reducing agents or contact with structural materials such as metallic alloys and graphite. The concept for the dynamic reference probe was originally proposed referenced from Afonichkin, et al, 2009 [45].

Prior to starting corrosion tests, FLiBe salt redox potentials are characterized by the dynamic Be-reference probe shown in Figure 4-1. The redox potential of unreduced as-purified UW Madison FLiBe is -1.71 V +/- 0.02 V, whereas the redox potential of the Be-reduced and filtered UW Madison FLiBe is -1.45 V +/- 0.03 V. Once the corrosion test is initiated, salt redox potential will equilibrate with the samples it is in contact with through corrosion mechanisms. At the end of the trial, the salt will have its redox potential and composition characterized to quantify any chemical changes in the environment.

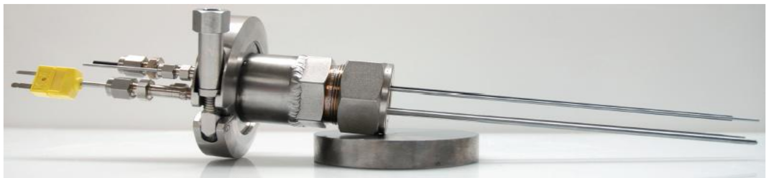

Figure 4-1. UW Madison dynamic reference electrode probe

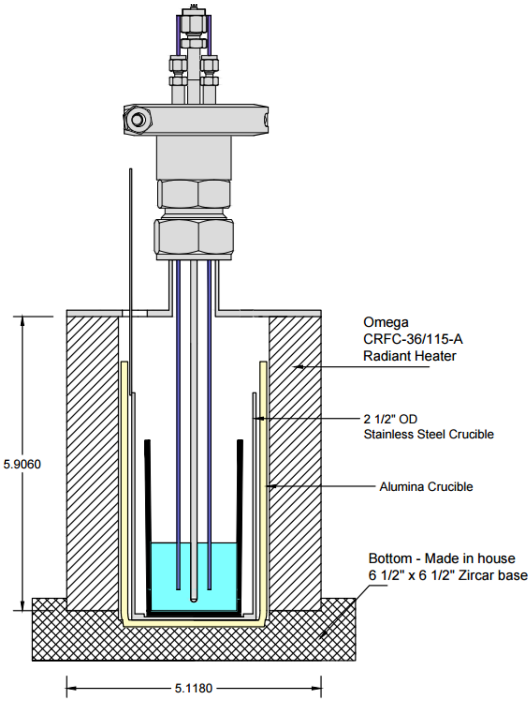

Figure 4-2. Electrochemical probe setup for measuring redox potential of molten FLiBe salt

4.1.2 **Reduction of FLiBe**

4.1.2.1 Beryllium Addition

Preparation of reduced UW Madison FLiBe consisted of 0.5 mg Be metal additions to 50 g batches of FLiBe. The FLiBe salts to be used in future corrosion studies will be purified in unreduced and Be-reduced states which constitutes a difference of 282 mV in redox potential. These salts have already been prepared and photograph of the salts is shown in Figure 4-3.

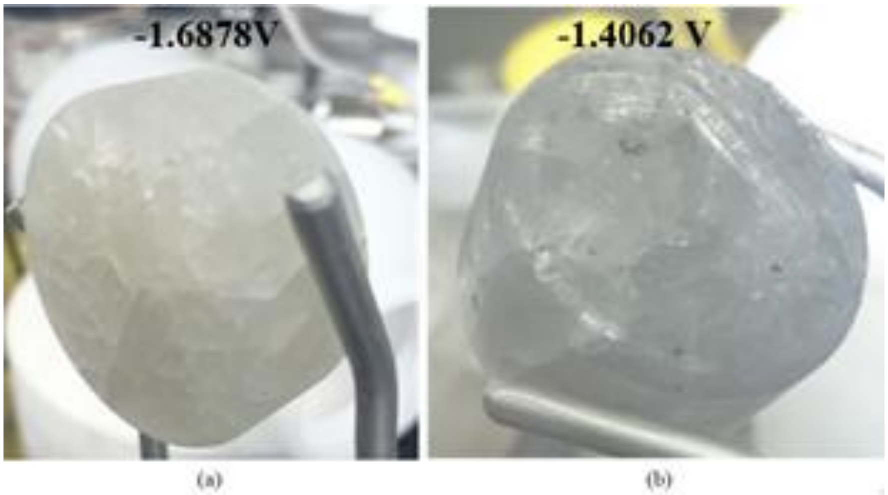

Figure 4-3. Unreduced (a) and reduced (b) variants of UW Madison raw-materials FLiBe

Salt was reduced by adding a 0.5 mg Be metal to four 50 g melts and allowing to dissolve for at least 24 hrs. A total of 200 g of FLiBe has been Be reduced for corrosion testing.

4.1.2.2 Electropurification

Using electrochemical salt reduction methods could mitigate the need for Be metal addition and potentially offer the benefit of a quick and *in situ* process for salt chemical control. Much like the redox potential measurement, impurities can be plated on to an electrode which can be removed from the salt. By plating potentiostatically for various periods of times at a potential slightly more positive than that of beryllium's reduction potential in FLiBe salt, a reduction of the salt was achieved. In a 30-minute test, the redox potential was increased by 172 mV. Evidence of impurity reduction onto the nickel coil cathode was also observed. Unfortunately, the glassy carbon anode introduced carbon into most electropurified FLiBe samples [46]. Future work on electropurification will likely revolve around identifying a superior anode material for electroplating in FLiBe. Cyclic voltammetry will be employed to study the presence of contaminants in FLiBe samples.

4.1.3 **Oxidation Tests of FLiBe**

The UW Madison dynamic reference electrode probe has been used to quantify the effect of dissolved corrosion impurities in FLiBe salt on the redox potential, a laboratory measurable voltage which indicates the tendency for constituents of the salt to undergo an oxidation or reduction reaction. A change in the redox potential signifies a change in the relative equilibrium of all reactions in the salt. In the pure state, the constituents of LiF-BeF_2 (66 – 33 mol %) are very chemically stable and thus reducing. The introduction of moisture into the system, however, leads to the formation of less stable hydrogen fluoride. The transfer of electrons from a stable cation to a less stable cation is an oxidation of the salt that makes the salt less compatible with alloying metals. The corrosion of alloying metals also leads to the formation of less stable fluorides in solution [47]. The goal of this work was to demonstrate the sensitivity of the redox potential measurement to the addition of roughly 250 ppm of nickel, iron and chromium fluorides to separate batches of FLiBe. It was demonstrated that both nickel and iron fluoride have an oxidizing effect that was measurable with the redox potential test [46]. This oxidizing behavior theoretically could significantly increase corrosion rate in the salt. While nickel and iron show somewhat reproducible oxidation behavior, more work is required to quantify the oxidizing effect of chromium which exhibited a response smaller than the error of the redox measurement. Further efforts to characterize these impurities may be carried out using alternative electrochemical techniques such as cyclic voltammetry.

4.1.4 **Ni/Ni(II) Reference Electrode**

Electrochemistry offers a wide range of well-established techniques to approach chemistry studies, but a thermodynamically stable Reference Electrode (RE) is needed to successfully employ several of those techniques. Commercially available RE made of borosilicate glass or other oxide containing ceramics cannot be used in fluoride salt due to their chemical instability in such environment. Ongoing research efforts at UW Madison are focused on the development of a thermodynamic stable reference electrode.

Several thermodynamic RE based on the Ni/Ni(II) redox couple were developed and tested in previous literature [48–50]. The Ni/Ni(II) redox couple showed Nernstian behavior [48] and the good polarizability behavior to be used as a reference reaction for a reference electrode. The literature still reports problems related to wettability time for the electrodes, cracking of materials and degradation over freezing/melting cycles.

The design of the thermodynamic RE under testing at UW Madison uses the LaF_3 ionic membrane presented Bronstein and Manning [49]. Some simplifications in these design were made, following similar design by Dr. Martin Straka [51]. A 35 mm tall, 10 mm outside diameter boron nitride one closed end tube is used for the electrode body. A LaF_3 single cylindrical crystal of diameter 6 mm and 5 mm tall is used as ionic membrane and placed at the bottom of the boron nitride tube. A hole of 0.3 mm diameter into the boron nitride tube provides contact between the crystal and the main salt batch (Figure 4-4. LaF_3 membrane reference electrode under testing at UW Madison. The RE utilizes the Ni/Ni(II) redox couple as a reference. A high purity nickel rod (4N purity, ESPI metals) of 0.0125 inches diameter is used as electrode. Approximately 1 gram of FLiBe salt is added to the boron nitride tube; NiF_2 is then added until the desired molar fraction is reached. Blood reports solubility limits for NiF_2 in FLiBe salt as a function of temperature [52].

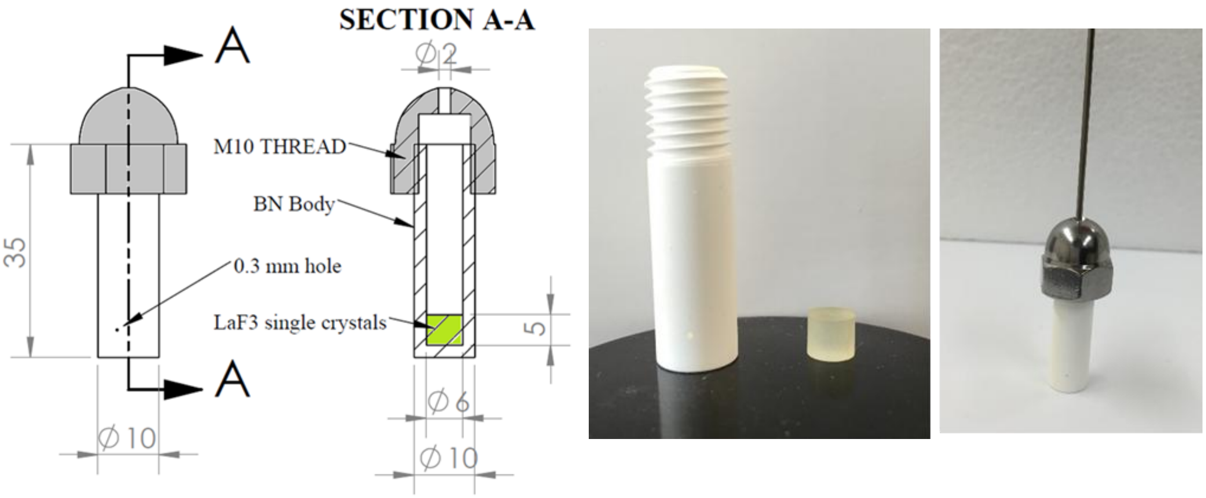

Figure 4-4. LaF_3 membrane reference electrode under testing at UW Madison

The electrode is currently under testing at UW Madison using both FLiBe and FLiNaK salt. Preliminary testing in FLiBe demonstrate a very low noise of the potential signal and a good short term stability. Long term stability still needs to be assessed. In FLiNaK however, the LaF_3 crystal used as a membrane shows a big corrosion attack.

4.1.5 **Tritium Transport with Electrochemistry**

Hydrogen transport has been intensively studied for water metal systems. Electrochemistry techniques employed to have an investigate diffusion and trapping of hydrogen in those aqueous system, including, potentiostatic double step method [53] and electrochemical impedance spectroscopy [54], can be used in a similar manner to study tritium transport in a fluoride molten salt system. Those techniques, supported by a coherent physical modelling, can be used to calculate experimentally tritium transport metrics in the fluoride melt, in the salt to graphite interface and inside the graphite.

4.1.6 **Solubilities, Diffusion Coefficients, and Transport of Species in Salt**

Transport of species in the salt has been identified to be an important phenomenon not just for tritium, but also for other elements like impurities and corrosion products, redox control species and activation products. For example, understanding how the redox control agent (beryllium) diffuses through the system is crucial into designing a redox control system. Solubility variation as a function of temperature in the primary loop can determine the deposition of corrosion and activation products in the cold leg.

The redox potential of the salt can play a role also in solubilities and transport of elements in the reactors, determining the equilibrium between the oxidation states of every element and form of this elements. Solubilities and diffusion coefficients of elements of interest can be calculated using electrochemistry techniques.

4.1.7 Redox Control Species, Corrosion Products, and Tritium

Using a molten fluoride salt coolant, such as FLiBe or FLiNaK, creates the significant challenge of minimizing corrosion of the system's boundary materials. This corrosion can be quantified from the "redox condition" of the salt, which is defined by the fluorine potential [55]. Methods such as HF/H_2 sparging, metallic beryllium contact, and cathodic protection have been proposed and tested to varying degrees for redox control of FLiBe [56].

To implement any redox control, a measurement system must first be developed. The development of an electrochemical measurement system has been identified as an important task for FLiBe redox control [57]. Such a measurement system would allow for the determination of the fluorine potential, an important factor in system health. This measurement system would implement cyclic voltammetry to acquire the peak voltage over the scan range. The value could then be used to calculate the concentration of the fluorine species in the solution using the Nernst equation.

A typical three-electrode system is used. Materials for the counter and working electrodes include tungsten, molybdenum, carbon, platinum, and others. No major problems are reported relating to the selection or use of these materials for the counter and working electrodes. The selection of the reference electrode is more difficult. The literature reports varied reference electrode selections with varying degrees of success.

Characteristics for identifying an appropriate reference electrode include the reversibility of the electrode system, stability and reproducibility of the potential, stability of the reference electrode materials, impedance of the reference electrode, and compatibility of the reference electrode with the type of measurement [57]. These characteristics should be used to analyze the usefulness of a reference electrode with an emphasis on stability of the potential and stability of the electrode materials, as these characteristics most pertain to the requirements of this application.

Platinum, among other metals, can serve the function of the reference electrode in an electrochemical cell for molten fluoride salt applications. Platinum has been used/proposed many times in the literature and appears to be becoming the preferred reference electrode in these systems due to its simplicity [58–61]. This type of reference electrode has been shown to be reversible, however platinum does not have a defined potential. Its potential reaches steady state within minutes but potential drift has been observed by experimenters ranging from 1-20 mV within a few days. This application requires better accuracy and stability over time requiring a reference that possesses a defined electron transfer reaction.

The Ni/Ni^{2+} reference electrode has been widely used as well in the literature [58]. The Ag/Ag^{+} electrode is commonly used for chloride salts and has also been used less so in fluoride salts. The Be/Be^{2+} electrode is also reported for fluoride salts which have beryllium constituents such as FLiBe [58]. This electrode is reversible and possesses a stable potential varying by 0.1 mV at 500-900 Celsius [59]. Each of these possible redox couples that act as reference electrodes have a common issue in the material stability used to separate the reference electrode compartment from the bulk salt. A few of these containment materials currently under study include boron nitride, graphite, and lanthanum fluoride [58]. The stability of nickel or silica as a construction material is not an issue. Impedance is not reported. This electrode is also compatible with cyclic voltammetry.

A unique dynamic electrode has been reported recently by Afonichkin for use in fluoride molten salts which contain BeF_2, such as FLiBe [45]. This design is relatively simple; which uses the Be/Be^{2+} reference electrode. The ion transfer diaphragm is eliminated by passing current pulses through the dynamic reference electrode which was selected to be a molybdenum wire. This causes beryllium to plate onto the wire allowing for a potential measurement to take place after which the potential is allowed to relax before repeating. Testing this electrode for reversibility was not reported, however a stable potential was identified over a period of 1200 hours at 700 Celsius. Over this period the potential varied by 5 mV. Stability of construction materials is not an issue the reference electrode is very simple, possessing no container or diaphragm. No impedance information was reported. This type of reference electrode is compatible with cyclic voltammetry while beryllium is plated onto the electrode.

For an industrial application, an electrochemical sensor will be required to maintain as much durability and service life as possible to avoid high operation costs. Therefore, the stability and reproducibility of potential and the stability of its materials will be the most important characteristics by which to compare. This burden is primarily placed upon the reference electrode as the limiting component in any proposed electrochemical cell. Very few studies have reported the results of potential stability over the course of a time scale appropriate for industrial application and only one was tested in a convection loop for validation in such an environment. The electrodes above are the most promising reference electrodes for this application. Further research will be conducted to properly analyze and compare the reference electrode types and construction to determine an ideal recommendation for an electrochemical sensor design for use in FLiBe and FLiNaK.

Since the oxide layer becomes unstable and non-protective in high-temperature fluoride salts, the redox potential must be controlled in a certain range for mitigating corrosion of the structural alloys. Zr has been recognized as a strong reductant, and is one of the candidates for redox control in fluoride salts. Preliminary calculation using published electrode standard potentials has been performed, and the results show that the concentration of dissolved Ni, Fe, and Cr can be limited to very low levels by controlling the Zr^{4+} concentration in the salt at 750 °C. More reliable standard potentials and thermodynamic data will be find from published source or from own experiments. Efforts will also be made to look for other candidates for redox control in fluoride salts. The redox control using Zr/Zr^{4+} will be verified by comparing the series C200 corrosion tests and the series C100 corrosion tests.

Tritium will exist in the FHR in the form of either dissolved ions (T^+), dissolved tritium gas (T_2 or HT), or tritium fluoride (TF) which is very toxic and corrosive. Controlling the redox potential of the primary salt to a more reducing condition will shift the tritium equilibrium away from tritium fluoride. It has been shown previously that contacting the molten salt with beryllium can effectively reduce TF to T^+ in FLiBe [62]. Providing excess beryllium to the salt can lower the concentration of TF in the FLiBe to an estimated 20 ppt [63].

4.1.8 **Other Electrochemistry Open Questions**

Some material and chemistry related question have to be answered regarding chemistry and electrochemistry of molten salts.

- Moving forward what is the best way to produce high purity FLiBe? Is it starting from BeF_2 (used in the UW Madison FLiBe purification process) or BeO (used in SINAP process)?
- What are the best material to be used in contact with fluoride salts? Can Alumina be used as a possible acceptable material?
- What material should we use as a counter electrode? During reduction of impurities, the counter electrode reaction will be dissolution of this material or production of fluorine gas?
- The impurities plated in at the working electrode will carry a lot of salt constituents with them (around 80% of the elements collected where mentioned to be salt constituents). How can we make the process more efficient?

4.2 **Salt Spectroscopy**

Spectroscopy is an analytical tool used for the identification and determination of solute species in the solution. Such studies can be applied to molten fluoride salts, for the identification of ionic species in the melt by studying *in-situ* chemical equilibria of species, analogous to aqueous systems. The spectra of solute species in the melt can contribute much more than the analytical knowledge to the understanding of the structure and dynamics of fluoride salts. A detailed understanding of chemistry of salts is important for investigation of the salt-graphite interface for the FHR reactor design. With spectral studies, the mechanism of tritium transport and salt intrusion into the pores of matrix graphite, can be investigated. These studies can also lead to online/in-situ monitoring of any impurities and/or corrosion products present in the coolant.

The spectroscopy study of fluoride salts, however, is quite challenging in practice. The major challenge is the design of holder for the melts. The material under consideration should be able to withstand high temperatures, should be resistant to corrosive nature of fluorides, in addition to being transparent over a wide spectral range.

Several designs have been proposed over the years to accommodate these challenges, including windowless or captive cells [64] and diamond windowed graphite cell [65]. The report published by ORNL in 1967 discusses various options for windowless containers, however, there are several challenges associated with each design. For example, the use of screens might lead to inaccuracy in path length measurements. The use of reflection cells offer the analysis through the beam reflected from the mirror surface present at bottom of container. However, corrosion of liquid-mirror surfaces pertains to the possibility of large light scatter at the interface. Another approach is the use of optical material windows that are corrosion-resistant and can withstand high temperatures. Various options considered for optical windows are – noble metals coated quartz, sapphire and diamond. In addition, LiF , CaF, and MgO, are inexpensive optical materials with excellent transmission character, and can be considered for use as window for transmission spectroscopy of fluoride salts [64]. Later in 2000s, use of fiber optic technology for high temperature UV-Vis spectroscopy with molten salts was suggested by Cho and Jurovitski [66,67].

An interesting concept was discussed by Young in 1959, termed as pendent drop method. The idea is to suspend a drop of molten salt from a rod such that the drop is positioned in the focal plane of the light beam. Pendent drops nearly eliminate corrosion of the cell, which makes them advantageous [68]. Although these techniques present some favorable attributes, there are still certain challenges associated with the design of materials considered for molten fluoride salt spectroscopy that leads the quest to further investigate potential cell materials stable under extreme conditions.

At UW Madison, research has been carried out to design efficient holders for spectroscopic analysis of fluoride salts. The techniques such as, UV-Vis spectroscopy, diffuse-reflectance FTIR, high temperature NMR and Raman spectroscopy will be applied in order to better understand the fundamental chemistry of FLiBe and on line monitoring of certain species (impurities and corrosion products). In addition, the salt intrusion mechanism through the salt-graphite interface will be investigated using spectroscopic techniques such as in-situ Raman spectroscopy.

4.3 Beryllium Safety

To make the FHR commercially viable, industrial-scale beryllium hygiene procedures must be developed. The first step to doing this is to develop laboratory-scale beryllium hygiene procedures that meet current beryllium hygiene standards. OSHA has set limits of 0.2 $\mu g/m^3$ of beryllium in a 8 hours' time-averaged sample of the room atmosphere [69]. For detecting surface beryllium contamination, the Department of Energy recommended action limit is 0.2 $\mu g/100cm^2$ [70].

To monitor for these action levels and measure personnel exposure, a series of beryllium monitoring practices are employed at UW Madison. Periodic air monitoring and laboratory swipe tests are conducted, and they are conducted during and after high-risk beryllium activities such as transferring contaminated material outside of glovebox containments. All personnel are subjected to annual beryllium blood tests as well as optional chest x-rays to monitor personal exposure. The blood test can be an indicator of increased beryllium sensitivity, one of the symptoms of beryllium exposure. Additionally, all personnel conduct an annual respirator fit test and breathing performance test to complement the beryllium monitoring. The breathing test can be an indicator of the onset of breathing difficulty, one of the symptoms of beryllium exposure.

To prevent beryllium exposure, a variety of strategies are employed by UW Madison. Most beryllium work is conducted in gloveboxes in order to keep the FLiBe chemically pure as well as to provide a protective barrier between beryllium and personnel. Chemical goggles, nitrile gloves, lab coats, close toed shoes, and long pants are all used when working with beryllium to minimize skin contact in the event of beryllium contamination outside the glovebox. A respirator is available for personnel use for high-risk beryllium activities such as transferring contaminated material outside of glovebox containments, or in case of glovebox containment failure. Another location beryllium work is conducted is in a walk-in fume hood. For work done in the fume hood, a respirator and full body hazardous materials suit are used to minimize personnel exposure.

Beryllium disposal and decontamination are also key components of the laboratory hygiene plan at UW Madison. Liquid beryllium waste such as contaminated water is labeled in a sealed container and sent to the campus chemical disposal service. Solid beryllium waste such as used FLiBe is also labeled in a sealed container and sent to the campus chemical disposal service, though minimal FLiBe is disposed of due to material scarcity. Material that is contaminated by beryllium such as gloves and wipes are placed in specially-marked, double-layered bags before being placed directly into university trash receptacles. Other options such as direct disposal off-campus are being explored to further reduce general population beryllium exposure.

4.4 Benchmarking

4.4.1 Spectroscopy Techniques

The estimation of spectroscopy data from any technique (UV-Vis, FTIR and Raman spectroscopy) can be performed by examining and comparing the spectra of standard fluids or materials under similar conditions. The materials standard for each technique should be specified and benchmarked. The materials used for both optical windows and containers (for transmission mode and reflectance mode) needs to be benchmarked. Other important parameters for spectroscopy are the pathlength and focal distance, for which benchmarking specifications for needs to be ascertained.

4.4.2 Beryllium Safety

The periodic beryllium monitoring practices (air monitoring and laboratory swipe tests) need to be benchmarked to maintain the beryllium levels below OSHA and DOE limits. In addition, proper Beryllium decontamination procedures need to be followed.

4.5 **Conclusions**

Salt chemistry strongly affects fluoride salt behavior in terms of corrosion, material transport, and physical properties. Monitoring the quality and redox potential of the salt and being able to maintain acceptable salt purity during the reactor lifetime is crucial for the success of a fluoride salt cooled reactor.

The dynamic reference probe developed by the Sridharan group is used to measure the redox potential of the salts and is able to sense the effect of oxidizing impurities (Ni, Cr, and Fe) and reducing Be metals introduction in pure FLiBe. Electro-purification appears as a viable way to purify the salt, and a proof of concept was shown. Several other electrochemistry techniques could be used to characterize molten salt system behavior in terms of solubilities and transport of different species, like redox control species, corrosion products, and activation products; to perform some of those techniques, a thermodynamically stable reference electrode is needed. A Ni/Ni(II) reference electrode was presented and is under testing at UW Madison.

Spectroscopy can be also used to monitor chemistry of the salt and to study salt properties. Optical absorption spectroscopy of molten fluoride salts can be used for the identification and quantitative determination of impurities and corrosion products in the melt by investigating in-situ chemical equilibria of the species. At UW Madison, we are designing an experimental setup to characterize the optical and vibrational states of FLiBe in order to yield important data for radiative heat transfer. The results from the spectroscopic analysis will be used to better understand the fundamental chemistry of FLiBe and analyze the corrosion behavior of FHR structural materials.

Be safety reported the procedures used at UW Madison to safely work with FLiBe and other Be-containing salts in a laboratory environment. Furthermore, it was remarked how the experience gained in dealing with Be in laboratory environments could be very valuable for the development of procedures and safety limits for personnel exposure in an FHR power plant.

5 Corrosion

5.1 Static Corrosion experiments

Static corrosion experiments have been and are being conducted at UW Madison and the OSU. Much of the work focuses on static corrosion testing carried out in carefully controlled glovebox environments to ensure reproducibility. Preparations for corrosion testing under flow are ongoing with the construction of a molten salt flow loop.

5.1.1 Redox Potential and Graphite Presence Corrosion Studies

Static corrosion testing to be completed at UW Madison during the summer of 2016 will be done using LiF-BeF_2 made from raw ingredients at UW Madison. Two varieties of salts will be investigated: 1. As-purified, unreduced, H_2/HF sparged and filtered, and 2. same starting salt with additional reduction with beryllium metal additions and subsequent filtration.

The currently planned static FLiBe corrosion test will focus on testing the following effects in two identical graphite crucibles:

1. Redox potential on corrosion in FLiBe
2. Presence of graphite on corrosion in FLiBe

Part of the FLiBe batch that was produced from raw materials and purified with HF/H_2 sparge will be used in one crucible of the planned corrosion test. This salt has a well-characterized redox potential of -1.706 V, and will serve as the baseline salt for comparison. The other crucible (identical sample arrangement) will contain a filtered, Be-reduced FLiBe that will be reduced by adding stoichiometrically equivalent Be(s) to replace impurity fluorides estimated from NAA. The goal of the experiment is to compare corrosion behavior of new and conventional samples as a function of redox potential.

Conventional materials tested previously include 316 Stainless Steel, CVD SiC, and nuclear graphite. New materials for testing in FLiBe include a Mo-Hf-C alloy sourced from H.C. Starck, a SiC-coated SiC-SiC composite sourced from General Atomics, and a W/ZrC Cermet sourced from Georgia Tech. Graphite samples to be tested in redox condition corrosion test include A-3

Matrix Graphite, and IG-110 Nuclear Graphite. The crucibles that contain salt and samples for corrosion testing are produced from IG-110 nuclear graphite. The new materials are listed in Table 5-1.

Table 5-1. Potential FHR-relevant materials for next phase of static corrosion testing using FLiBe

Material	Location	Supplier/ Manufacturer	Attractive Properties and Motivation	Compatibility with FLiBe
SiC-coated SiCm-SiCf Composite	Fuel cladding	General Atomics – Bob Schleicher	Improved fuel cycle and lower fuel costs for FHRs using SiC clad pellet fuel over TRISO fuel; high temperature irradiation resistance and strength	Shows good compatibility with CVD SiC, but composites depend on manufacturing process
Joined SiC-SiC Composite	Heat exchanger	CoorsTek/ Ceramatec – Charles Lewinsohn	Unique SiC-SiC joining technique	Composites expected to perform well
Graphite A3 (Matrix) and IG-110 (Nuclear)	Core structure	MIT	High temperature stability and strength	Chemically inert to FLiBe, but may have issues with high Be content in salt
Ho-Hf-C alloy	Control rod	H.C. Starck – Chip Urban	High temperature stability and strength	Mo inert in FLiBe; minimal corrosion expected
ZrC/W Cermet	Valves and sensors	Georgia Tech – Ken Sandhage	Good thermal shock resistance; easy to form into large complicated shapes	W inert in FLiBe; minimal corrosion expected

Sample preparation of the above samples is being carried out at present. Table 5-2 shows the experimental setup of the planned corrosion test. Additionally, a drawing and table showing the samples and their locations is shown in Figure 5-1.

Table 5-2. Experimental setup of next phase of static corrosion testing in FLiBe

Crucible 1: -1.69V UW Madison FLiBe	**Crucible 2: -1.45V UW Madison FLiBe**
Hole 1: SiC materials. 1x General Atomics polished and coated SiC-SiC 1x CoorsTek bonded SC-30 SiC-SiC 1x Ceramatec bonded CVD SiC	
Hole 2: C materials. 2x A3 matrix graphite sample 2x IG-110 nuclear graphite sample	
Hole 3: Mo-Hf-C. 3x Mo-Hf-C alloy samples with Mo wire suspension, no liner.	
Hole 4: W-Zr-C. 3x W-Zr-C Cermet samples with W wire suspension, no liner.	
Hole 5: 316 SS. 3x 316 samples with SS wire suspension, no liner.	
Hole 6: 316 SS. 3x 316 samples with SS wire suspension, with 316 SS liner.	

*Avoid dissimilar materials in contact in FLiBe wherever possible

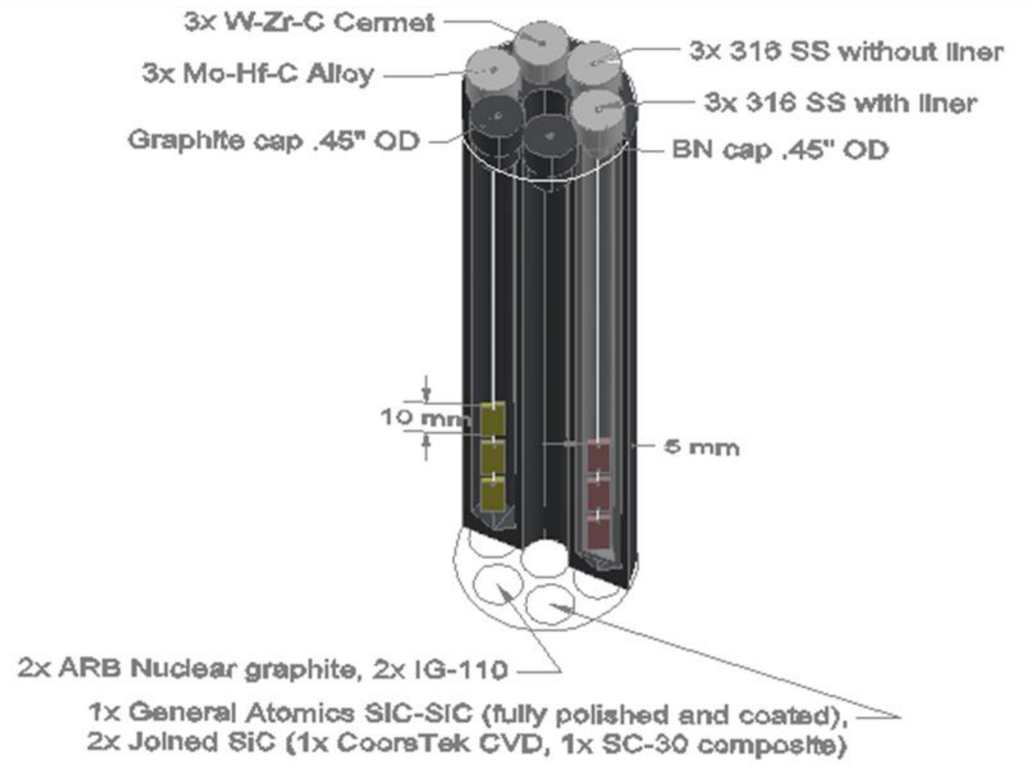

Figure 5-1. CAD drawing of corrosion crucible and sample locations

In this setup, metallic samples will be suspended with wire, whereas ceramic samples will be placed in the crucible freely. A total of about 150g of FLiBe per crucible is required. Figure 5-2 shows the two varieties of FLiBe salt made at UW-Madison that will be used for the static corrosion test.

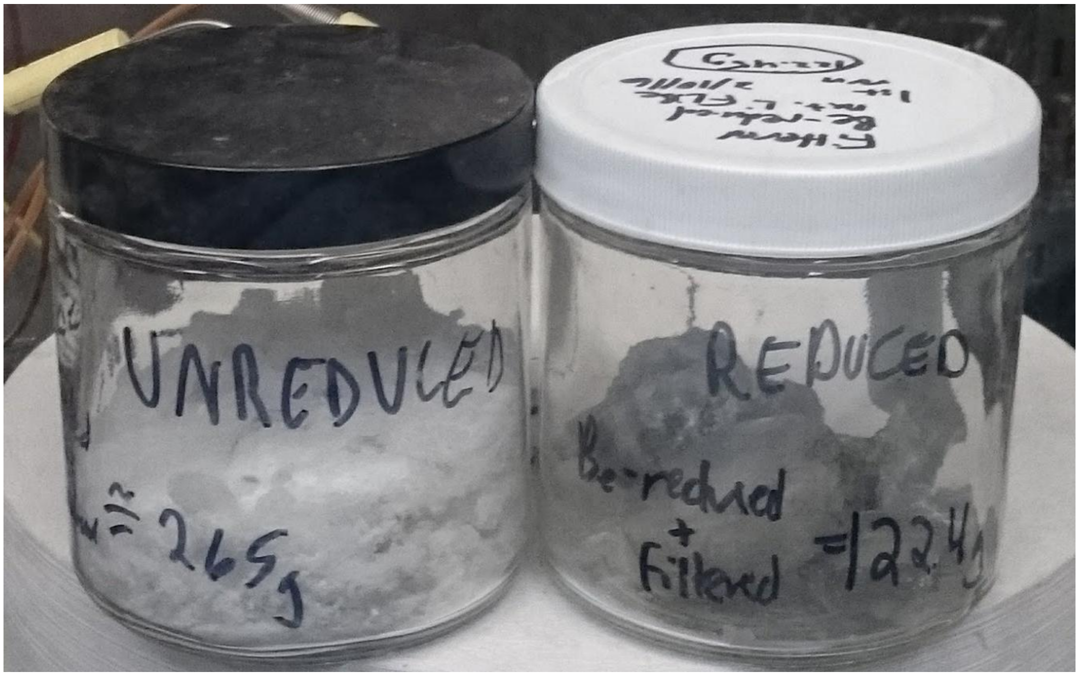

Figure 5-2. FLiBe salt to be used in static corrosion tests

Once all samples are fully prepared, corrosion crucibles will be filled with respective salts and covered with graphite plugs. The temperature of FLiBe for the corrosion test will be 600 ˚C, with an exposure time of 1000 or 2000 hours.

5.1.1.1 Procedure for Corrosion Tests

Crucible filling will be done inside of an atmosphere controlled glovebox with salt in a solid form. This will be accomplished by first carefully crushing the salt in a steel mortar and pestle to obtain a granulated consistency. Then, salt will be deposited into each 0.405” diameter hole with samples either hung on wires or resting in the bottom of the crucible. Once solid salt is filled to the top of each hole in the crucible, it will be moved into a heater to melt the salt. It is expected that the volume of the liquid salt will be much less than solid, so a loss of salt height is expected. In order to combat this issue, samples will be hung near the bottom of the crucible so that it is guaranteed that they will be submerged in the salt. In the case that samples are not fully submerged following the melting step, more granulated salt will be carefully added to the hot crucibles to raise the salt level. It is anticipated that this step will require dexterous handling in a glovebox.

Once the salt is filled and samples submerged to satisfaction, the heaters will be ramped up to the desired temperature of 600ºC and monitored for 1000 hours. During this time, additional samples will be characterized in optical microscopy as well as electron microscopy to observe the surface microstructure and topography, chemical composition, and overall appearance. In addition, all samples will be carefully weighed prior to adding to crucibles in order to monitor weight changes due to corrosion mechanisms. Additionally, surface hardness measurements will be take of all samples before and after corrosion to observe changes in mechanical properties in the structural material.

Pre-corrosion characterization of the materials in the test has begun, however multiple hurdles had to be crossed. First and foremost was the cutting of holes in composite and refractory metal samples for hanging in the crucible. Since W-Zr-C cermet samples are too hard to drill with conventional bits, EDM or diamond drill bits are required to cut holes into the samples, which caused a delay in preparation. Also, the W-Zr-C samples were found to be too porous for proper corrosion testing, so a new set of fully dense samples had to be delivered. Lastly, the Mo-Hf-C samples suffer a similar fate due to the fact that the samples contain carbides that increase the hardness substantially. These materials will need to be polished with diamond grinding pads to a 1200 grit finish to obtain a surface that is satisfactory for cross sectional analysis and accurate corrosion rate measurement.

5.1.1.2 Materials Analysis Techniques

Characterization of the samples before and after exposure to FLiBe will include optical microscopy, SEM/EDS, and XRD. All samples will be flat polished to 1200 grit using metallographic SiC polishing papers prior to all characterization and corrosion testing.

Post corrosion weight change will be a major component of corrosion analysis for various samples. In addition, surface and cross section morphology and compositional changes will be analyzed with SEM and EDS. This technique can also show chromium depletion depth, which is an indication of attack depth.

5.1.2 **Corrosion Behaviors of Alloys in FLiBe and FLiNaK**

The corrosion behaviors of various alloys including Hastelloy N, Ni-201, Incoloy 800, stainless steel 316L will be investigated at OSU. A literature review of electrochemical measurement techniques used in molten salt corrosion, current method used for studying the corrosion in molten fluorides salts and progress was performed in order to develop experimental procedure and better design the test plan.

A high temperature electrochemical cell has been fabricated and moved inside the glove box for corrosion testing. The water vapor concentration and oxygen concentration are controlled by purging the glovebox with argon. A KERR Electro-Melt furnace is used to melt the salt and control the salt temperature. A typical 3-electrode electrochemical cell is designed where a graphite rod is used as the counter electrode, a platinum wire is used as the reference electrode, and the rod test material will be used as the working electrode. A Gamry Interface 1000 potentiostat with the Gamry Framework software will be used for various electrochemical measurements. The potentiodynamic polarization curve will be used to get the instantaneous corrosion rate (corrosion current density), corrosion potential and Tafel slopes. Electrochemical impedance spectroscopy will be used to characterize the resistance the oxide film may be formed on metal surface and the charge transfer resistance. The evolution of open circuit potential with time will be used to monitor the growth and breakdown of the formed oxide film. The composition of the salt before and after the test will be examined by inductively coupled plasma

(ICP) analysis. The surface and cross-sectional morphologies of the samples will be observed using scanning electron microscopy (SEM), and the composition will be analyzed by energy dispersive spectrometry (EDS), X-ray diffraction (XRD) and X-ray photoelectron spectroscopy (XPS). The test duration is 24 hours, and the temperature is 700 °C. Table 5-3 shows the test matrix and current status for the baseline corrosion test, which is named as series C100.

Table 5-3. Test matrix for series C100 and test status

Test #	Material	Salt	Measurements	Status
C101	Hastelloy N	FLiNaK	OCP, EIS, Polarization	Completed
C102	Hastelloy N	FLiNaK	OCP, EIS, ICP, XRD, Cross-section SEM	On-going
C103	SS316	FLiNaK	OCP, EIS, Polarization	Completed
C104	SS316	FLiNaK	OCP, EIS, ICP, XRD, Cross-section SEM	
C105	Ni-201	FLiNaK	OCP, EIS, Polarization	Completed
C106	Ni-201	FLiNaK	OCP, EIS, ICP, XRD, Cross-section SEM	
C107	Incoloy 800	FLiNaK	OCP, EIS, Polarization	Completed
C108	Incoloy 800	FLiNaK	OCP, EIS, ICP, XRD, Cross-section SEM	

Note: At least 1 replicate test will be designed for each test to make sure the data is reproducible.

After the validation of developed redox senor and the redox control simulation using Zr/Zr^{4+}, series C200 fluoride salts tests will be designed to investigate the corrosion behavior of various materials in different redox control condition. Those results will be compared with the series C100 test results. The fabrication of the exhausting system for the glovebox will be completed in 2 weeks. And series C300 will be designed to investigate the corrosion behavior of materials in FLiBe salts.

5.2 Dynamic Corrosion Experiments

To further qualify the materials that will be used in the FHR, UW Madison is constructing a molten salt thermal convection flow loop, shown in Figure 5-3. The loop is designed to have samples inserted and removed during operation from both vertical legs, through the two tanks.

Radiant mode heaters and annular forced- convection coolers help control the loop temperature and provide natural circulation driven flow at rates of around 5 cm/s, within the Reynolds number range of 200-800. The loop is instrumented with both wetted and surface thermocouples for temperature at various locations, and two redox probes to measure the salt chemistry in each tank. Additions of beryllium will be used to help control the salt chemistry, allowing several different sample trains to be tested under similar conditions.

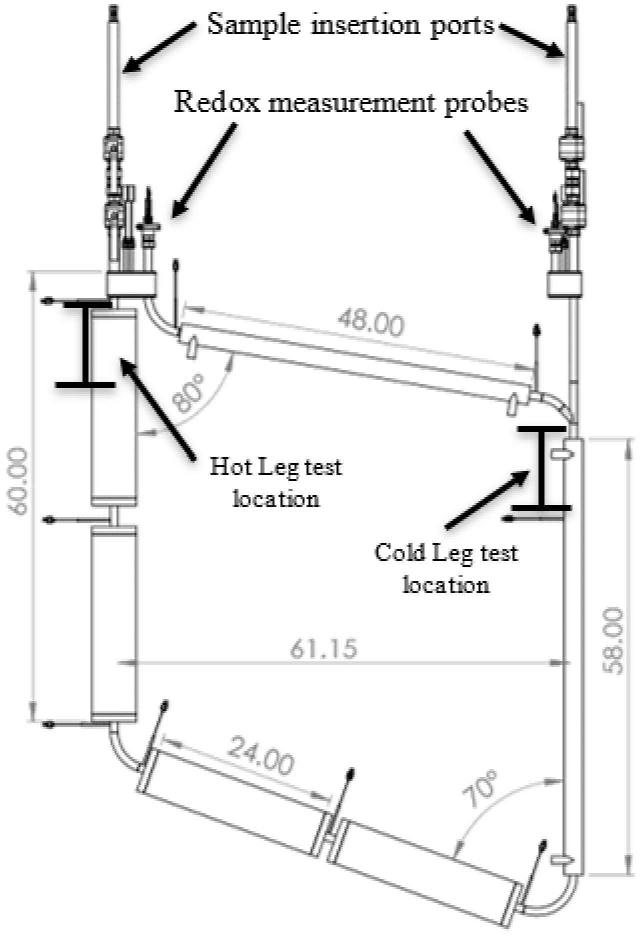

Figure 5-3. Flow loop, dimensions in inches

Loop testing will provide data on the weight-loss and depth of attack for materials used in the FHR; with early emphasis on type 316L stainless steel. Previous tests at UW Madison have quantified corrosion of SS 316L stainless steel under static environment, and comparison against dynamic corrosion data is necessary to better understand the corrosion mechanisms. The biggest difference between static and dynamic testing is the flowing salt alleviates concerns about mass-diffusion limited corrosion, providing constant mixing of fresh salt to limit the size of the diffusion boundary layer. Additionally, the temperature difference required for natural circulation provides two test locations with slightly different solubility for corrosion products, something that is expect to create a minor impact on corrosion.

The loop design is based off previous work during the MSRE, which found corrosion was most impacted by the difference between the temperatures of the sample and the salt; with hot steel suffering greater corrosion than cold [71]. The UW Madison Flow loop is designed to test samples in thermal equilibrium with the salt by using the sample trains shown in Figure 5-4, to provide a baseline corrosion rate that is comparable to the previous UW Madison static corrosion tests. However, simulations of the flow loop using ANSYS Fluent show a large temperature gradient across the radius of the pipe, resulting from the large heat loads and low thermal conductivity of the salt. It has not been determined how this thermal gradient will impact corrosion of the samples and discussions at the meeting focused upon the necessity of accurate flow field simulations around the sample train to better understand the thermal mixing and the mass-diffusion boundary layer development in the low Reynolds number flow.

Figure 5-4. Rendering of corrosion sample test train

5.3 Benchmarking

From the discussion about experimental chemistry, electrochemistry, and corrosion science, several areas that need benchmarking emerged and are considered in the following paragraphs.

5.3.1 Redox Measurements and Salt Purity

Experimentation with molten FLiBe salt is impacted by the chemical structure of the salt. Specifically, the salt redox potential and the salt purity are the two parameters that were considered as crucial for every set of experimental data. For the salt redox potential, or fluoroacidity, a standardized way of measuring it and to report it needs to be defined, to allow easy comparison between experimental conditions. Electrochemistry probes can be used to measure and report the redox potential; it would be interesting to benchmark different probes to verify an accurate reading of the redox potential and to finally establish the most reliable standard procedure to measure them. In regards to the purity measurements, an indication of impurities present in the salt needs to be added to experimental data sets. Currently, ICP-OES has been used to estimate the amount of impurities present in the salt.

5.3.2 Database for Chemical and Electrochemical Properties

It was discussed how it would be important, as the IRPs grow in number of groups and researchers involved, to develop a common database for chemical and electrochemical properties used to design and to model molten salts. The database could be public and could be shared with other interested MSR communities.

5.3.3 Metal Alloy Characterization Standards and Common Stock Material Procurement

Sample preparation and the sample manufacturing processes can have an impact on the results of corrosion and chemistry experiments. It is important to characterize any corrosion sample before an experiment and to define a common sample preparation procedure between different groups, to be able to directly compare data and results. The possibility of purchasing common stock of raw materials and sharing them between participating research institutes in the IRP was discussed as an important step for uniform and reproducible results.

5.4 **Conclusions**

To ensure the reliability of materials in contact with molten salts, both static and dynamic corrosion tests are being performed on a variety of materials. Static corrosion testing in glovebox focuses on carefully controlled salt chemistry to measure ideal corrosion rates and understand the basic mechanisms. A set of tests at UW Madison will examine the long-term corrosion, which occurs at different redox potential salts, while tests at OSU will examine the current densities related to corrosion metals. Dynamic corrosion testing attempts to overcome concerns about diffusion-limited corrosion reactions as well as provide a more flexible test bench, which allows salt chemistry to be tuned while the experiment is ongoing.

Conclusions and Path Forward

The present white paper summarized the discussions of MATT working group, as part of workshop 2 IRP-2 held at UC Berkeley from April 12-14, 2016. The MATT session was conducted in five sessions: Tritium modeling, Tritium control strategies, Tritium in Graphite, Salt Chemistry and Materials Corrosion. Each session was facilitated by students/researchers from the participating Institutes. The goal of each session was to discuss the various problems encountered by the researchers pertaining to FHR design and implementation. The discussion was further lead by experts in the field; the relevant comments and suggestions from the discussion are presented in each section. One major conclusion for each session was the pertinent need for various benchmarking parameters.

Chapter 1 discussed the modeling of tritium transport in the FHR core, where various parameters were used to calculate the tritium production rate. Primary tritium management strategy includes the investigation of tritium generation and absorption in graphite, to ascertain the limits of tritium release for FHR design. Models like TRIDENT and COMSOL are used to predict the tritium production values; and the results obtained are benchmarked against experimental diffusion data from fusion and previous MSR applications. Chapter 2 discussed multiple methods implemented to address the tritium challenge for FHR design. Various separation techniques were discussed in this chapter, alongwith the experimental and modeling benchmarks for each of the methods. Chapter **Error! Reference source not found.** discusses various challenges for investigation of tritium diffusion in molten salt-graphite system. Factors such as salt chemistry, microstructure of graphite, presence of other species (impurities or fission product), largely affect the diffusion of tritium into pores of graphite. The results from graphite microstructure analysis have been presented and correlated with the hydrogen diffusion in graphite and at graphite-salt interface to predict the mechanistic pathway of hydrogen transportation in FHR system. Chapter 4 demonstrates the effect of salt chemistry (purity and redox potential) on fluoride salt behavior considering corrosion, material transport and other physical aspects. The design and testing of dynamic reference probes developed at UW Madison, to carry out electrochemical reactions, have been presented. The electrochemical tools can be used to characterize molten salt behavior in terms of solubilities and transport of different species. In addition, the ongoing research on spectroscopy of FLiBe and salt-graphite interface carried out at UW Madison, has been discussed. The discussion on the procedures and principles used in practice for Be safety at UW Madison forms an important part of this section. Further in Chapter 5, the details of static and dynamic corrosion tests performed at UW Madison on a variety of materials are presented. Static corrosion tests include both short term and long term test, to measure ideal corrosion rates and understand the basic corrosion mechanism occurring at different redox potential salts. The discussion of ongoing dynamic corrosion testing setup to understand the basic mechanism of diffusion-limited corrosion reactions, is also included. The experiments carried out at OSU focus on examining the current densities related to metal corrosion.

References

[1] E. Forsberg, C. W., Lam S., Carpenter D. M., Whyte D.G., Scarlat, R., Contescu C., J. Stempien J., and Blandford, Tritium Control and Capture in Salt-Cooled Fission and Fusion Reactors: Status, Challenges, and Path Forward, Nucl. Technol. (n.d.).

[2] C. Forsberg, Basis for Fluoride-Salt-Cooled High- Temperature Reactors with Nuclear Air-Brayton Combined Cycles and Firebrick Resistance-Heated Energy Storage, 196 (2015) 22.

[3] M. Atlas, N. Brickner, W. Chen, D. Tsai, Tritium Management Approach for FHRs Using Supercritical Steam, Open-Air Brayton, and Closed Gas Brayton Power Cycles, 2012.

[4] A.T. Cisneros, Pebble Bed Reactors Design Optimization Methods and their Application to the Pebble Bed Fluoride Salt Cooled High Temperature Reactor (PB-FHR), University of California, Berkeley, 2013.

[5] R.B. Briggs, Tritium in molten-salt reactors, React. Technol. 14 (1972) 335–352.

[6] R.C. Robertson, Conceptual Design Study of a Single-Fluid Molten-Salt Breeder Reactor, Oak Ridge, TN, 1971.

[7] R.C. Robertson, MSRE Design and Operations Report Part I: Description of Reactor Design, Oak Ridge, TN, 1965. doi:10.1088/1751-8113/44/8/085201.

[8] D.T. Ingersoll, C.W. Forsberg, L.J. Ott, Status of Preconceptual Design of the Advanced High-Temperature Reactor (AHTR), Oak Ridge, TN, 2004.

[9] J.N. Rodriguez, Tritium Production Analysis and Management Strategies for a Fluoride-salt-cooled High-temperature Test Reactor (FHTR), Massachusetts Institute of Technology, 2013.

[10] C. Andreades, A.T. Cisneros, J.K. Choi, Technical Description of the "Mark 1" Pebble-Bed Fluoride-Salt-Cooled High-Temperature Reactor (PB-FHR) Power Plant, 2014.

[11] J.D. Stempien, Tritium Transport, Corrosion, and Fuel Performance Modeling in the Fluoride Salt–Cooled High Temperature Reactor (FHR), Massachusetts Institute of Technology, 2015.

[12] S.R. Sherman, T.M. Adams, Tritium Barrier Materials and Separation Systems for the NGNP, Aiken, SC, 2008.

[13] Management of Waste Containing Tritium and Carbon-14, Tech. Reports Ser. 421 (2004). http://www-pub.iaea.org/MTCD/Publications/PDF/TRS421_web.pdf.

[14] J.D. Stempien, R.G. Ballinger, C.W. Forsberg, A Model of Tritium Transport and Corrosion in Salt-Cooled Reactors John, in: 2015 Am. Nucl. Soc. Winter Meet., 2015: pp. 8–11.

[15] S. Fukada, A. Morisaki, Hydrogen Permeability through a Mixed Molten Salt of LiF, NaF and KF (FLiNaK) as a Heat-Transfer Fluid, J. Nucl. Mater. 358 (2006) 235–242. doi:10.1016/j.jnucmat.2006.07.011.

[16] J.R. Keiser, Compatibility Studies of Potential Molten-Salt Breeder Reactor Materials in Molten Fluoride Salts, Oak Ridge, TN, 1977.

[17] S.T. Lam, Tritium Management and Control Using Carbon in Fluoride Salt-Cooled High Temperature Reactors, in: ANS Tritium Conf., American Nuclear Society, Charleston, SC, 2016.

[18] L. Huddar, P.F. Peterson, Experimental Strategy for the Determination of Heat Transfer Coefficients in Pebble-Beds Cooled By Fluoride Salts, NURETH-16, Chicago, IL, August

30-September 4, 2015. (2015) 1659–1675.

[19] R.B. Lindauer, MSRE DESIGN AND OPERATIONS REPORT. PART VII. FUEL HANDLING AND PROCESSING PLANT, Oak Ridge National Lab., Tenn., 1965.

[20] J. Yin, J. Li, Y. Ma, H. Li, W. Liu, Study on the air core formation of a gas–liquid separator, J. (2015). https://energyresources.asmedigitalcollection.asme.org/data/Journals/JFEGA4/933887/fe_137_09_091301.pdf (accessed August 7, 2016).

[21] R.C. Robertson, J.L. Anderson, H.F. Bauman, C.E. Bettis, E.S. Bettis, R.B. Briggs, W.L. Carter, C.W. Collins, W.P. Eatherly, S.J. Ditto, W.K. Furlong, P.N. Haubenreich, E.C. Hise, P.R. Kasten, R.J. Kedl, H.E. McCoy, H.A. McLain, L.E. McNesse, J.R. McWherter, R.L. Moore, A.M. Perry, M.W. Rosenthal, D. Scott, W.H. Sides, A.N. Smith, O.L. Smith, J.R. Tallackson, R.E. Thoma, H.L. Watts, L. V Wilson, Conceptual Design Study of a Single-Fluid Molten-Salt Breeder Reactor, Oak Ridge, TN, 1971. http://web.ornl.gov/info/reports/1971/3445600591394.pdf.

[22] T.S. Kress, Mass Transfer Between Small Bubbles and Liquids in Concurrent Turbulent Pipeline Flow, University of Tennessee, 1972.

[23] J. Serp, M. Allibert, O. Benes, The molten salt reactor (MSR) in generation IV: Overview and perspectives, Prog. Nucl. Energy. 77 (2014) 308–319. doi:10.1016/j.pnucene.2014.02.014.

[24] M.W. Rosenthal, R.B. Briggs, P.N. Haubenreich, Molten-Salt Reactor Program Semiannual Progress Report for Period Ending August 31, 1970, Oak Ridge, TN, 1972.

[25] J. Hughes, Compact Double-Wall Twisted-Tube Heat Exchanger for the Fluoride Salt-Cooled High-Temperature Reactor (FHR) with Implications for In-Service Inspection, in: ANS Winter Meet., Anaheim, CA, 2014.

[26] L. Gilman, C. Forsberg, Optimum Double-Wall Heat Exchanger for Containment and Trapping of Tritium in a Salt-Cooled Reactor, in: Trans. Am. Nucl. Soc., Washington, D.C., 2013.

[27] D. Butterworth, A.R. Guy, J.J. Welkey, Design and Application of Twisted-Tube Exchangers, n.d.

[28] M. Ortman, T. Warren, D. Smith, No Title, Fusion Technol. 8 (1985) 2330–2336.

[29] M. Sharpe, C. Fagan, W.T. Shmayda, W.U. Schröder, Influence of Surface Roughness and Gold Plating on the Adsorption and Absorption of Tritium into Stainless Steel (Type 316), in: ANS Tritium Conf., American Nuclear Society, Charleston, SC, 2016.

[30] F. Rubio, E.D. Blandford, L.J. Bond, Survey of Advanced Nuclear Technologies for Potential Applications of Sonoprocessing, Ultrasonics. 71 (2016) 211–222.

[31] J. Yin, J. Li, Y. Ma, Study on the Air Core Formation of a Gas-Liquid Separator, J. Fluids Eng. 137 (2015) 1–9.

[32] K. Akita, F. Yoshida, Bubble Size, Interfacial Area, and Liquid-Phase Mass Transfer Coefficient in Bubble Columns, Ind. Eng. Chem. Process Des. Dev. 13 (1974) 84–91. doi:10.1021/i260049a016.

[33] A. Fadavi, Y. Chisti, Gas-Liquid Mass Transfer in a Novel Forced Circulation Loop Reactor, Chem. Eng. J. 112 (2005) 73–80.

[34] R.A. Causey, R.A. Karnesky, C. San Marchi, Tritium Barriers and Tritium Diffusion in Fusion Reactors, Compr. Nucl. Mater. 4 (2012) 511–549. doi:10.1016/B978-0-08-056033-5.00116-6.

[35] F. Reiter, J. Camposilvan, M. Caorlin, G. Saibene, R. Sartori, Interaction of Hydrogen

Isotopes with Stainless Steel 316 L, Fusion Technol. 8 (1985) 2344–2351.
[36] S.K. Lee, S.H. Yun, H.G. Joo, S.J. Noh, Deuterium transport and isotope effects in type 316L stainless steel at high temperatures for nuclear fusion and nuclear hydrogen technology applications, Curr. Appl. Phys. 14 (2014) 1385–1388. doi:10.1016/j.cap.2014.08.006.
[37] J. Kane, C. Karthik, D.P. Butt, Microstructural Characterization and Pore Structure Analysis of Nuclear Graphite, J. Nucl. Mater. 415 (2011) 189–197. doi:10.1016/j.jnucmat.2011.05.053.
[38] J. Landers, G.Y. Gor, A. V Neimark, Density Functional Theory Methods for Characterization of Porous Materials, Colloids Surfaces A Physicochem. Eng. Asp. 437 (2013) 3–32. doi:10.1016/j.colsurfa.2013.01.007.
[39] L. He, Y.B. Melnichenko, N.C. Gallego, Investigation of morphology and hydrogen adsorption capacity of disordered carbons, Carbon N. Y. 80 (2014) 82–90. doi:10.1016/j.carbon.2014.08.041.
[40] S. Lowell, J.E. Shields, M.A. Thomas, M. Thommes, Characterization of Porous Solids and Powders: Surface Area, Pore Size and Density, Kluwer Academic Publishers, Dordrecht, The Netherlands, 2004.
[41] H. Atsumi, T. Tanabe, T. Shikama, Trapping State of Hydrogen Isotopes in Carbon and Graphite Investigated by Thermal Desoprtion Spectrometry, Fusion Sci. Technol. 67 (2015) 245–249.
[42] X. Hu, E. Mangano, H. Ahn, Diffusion Mechanism of CO2 in 13X Zeolite Beads, Adsorption. 20 (2014) 121–135. doi:10.1007/s10450-013-9554-z.
[43] A. Snelson, The Reaction of Atomic Hydrogen with Carbon, Adv. Chem. Ser. 131 (1974) 54–71.
[44] K.H. Lee, S.J. Noh, B.S. Lee, S.J. Yoon, Solid-Vapor Equilibrium Phase Diagram of Hydrogen-Adsorbed Carbon, Langmuir. 16 (2000) 10184–10188.
[45] V.K. Afonichkin, A.L. Bovet, V. V. Ignatiev, Dynamic Reference Electrode for Investigation of Fluoride Melts Containing Beryllium Difluoride, J. Fluor. Chem. 130 (2009) 83–88. doi:10.1016/j.jfluchem.2008.07.017.
[46] K.P. Dolan, Redox Potential Measurement and Control for the Fluoride- Salt-Cooled High-Temperature Reactor, University of Wisconsin-Madison, 2015.
[47] B. Kelleher, Purification and Chemical Control of Molten Li 2 BeF 4 Salts for a Fluoride Salt Cooled Reactor, University of Wisconsin-Madison, 2013.
[48] H.W. Jenkins, G. Mamantov, D.L. Manning, EMF Measurements on the Nickel-Nickel II couple in Molten Fluorides, Eletroanalytical Chem. Interfacial Electrochem. 19 (1968) 385–389.
[49] H.R. Bronstein, D.L. Manning, Lanthanum Trifluoride as a Membrane in Reference Electrode for Use in Certain Molten Fluorides, J. Electrochem. Soc. 119 (1972) 125–128.
[50] C.G. Kontoyannis, Pyrolytic Boron Nitride Coated Graphite as a Container of Reference Electrodes for Molten Fluorides, Electrochim. Acta. 40 (1995) 2547–2551.
[51] M. Straka, M. Korenko, F. Lisý, Electrochemistry of uranium in LiF-BeF2 melt, J. Radioanal. Nucl. Chem. 284 (2010) 245–252. doi:10.1007/s10967-010-0478-8.
[52] C.M. Blood, Solubility and Stability of Structural Metal Difluorides in Molten Fluoride Mixtures, 1964.
[53] B. Pound, G. Wright, R. Sharp, A potentiostatic double-step method for measuring hydrogen atom diffusion and trapping in metal electrodes—II. Experimental, Acta Metall.

35 (1987) 263–270.

[54] M.E. Orazem, B. Tribollet, Electrochemical Impedence Spectroscopy, Wiley, Hoboken, New Jersey, 2008.

[55] D.R. Olander, Redox condition in molten fluoride salts: Definition and control, J. Nucl. Mater. 300 (2002) 270–272.

[56] D.E. Holcomb, G.F. Flanagan, G.T. Mays, Fluoride Salt-Cooled High-Temperature Reactor Development Roadmap, in: Int. Congr. Adv. Nucl. Power Plants, American Nuclear Society, Carlotte, NC, 2014.

[57] N.Q. Minh, L. Redey, Reference Electrodes for Molten Electrolytes, Molten Salt Tech. 3 (987) 105–287.

[58] M.M. Tylka, J.L. Willit, J. Prakash, M.A. Williamson, Method Development for Quantitative Analysis of Actinides in Molten Salts, J. Electrochem. Soc. 162 (2015) H625–H633. doi:10.1149/2.0281512jes.

[59] D.L. Manning, G. Mamantov, Rapid Scan Voltammetry and Chronopotentiometric Studies of Iron in Molten Fluorides - Fabrication and Use of a Pyrolytic Graphite Indicator Electrode, J. Electroanal. Chem. 7 (1964) 102–108.

[60] K.K. Kasem, S. Jones, Platinum as a reference electrode in electrochemical measurements, Platin. Met. Rev. 52 (2008) 100–106. doi:10.1595/147106708X297855.

[61] M.S. Sohal, P. Sabharwall, P. Calderoni, Conceptual Design of Forced Convection Molten Salt Heat Transfer Testing Loop, Idaho Falls, ID, 2010. doi:10.2172/1000546.

[62] D. a. Petti, G.R. Smolik, M.F. Simpson, JUPITER-II Molten Salt FLiBe Research: An Update on Tritium, Mobilization and Redox Chemistry Experiments, in: Fusion Eng. Des., 2006: pp. 1439–1449. doi:10.1016/j.fusengdes.2005.08.101.

[63] M.F. Simpson, G.R. Smolik, J.P. Sharpe, Quantitative Measurement of Beryllium-Controlled Redox of Hydrogen Fluoride in Molten Flibe, Fusion Eng. Des. 81 (2006) 541–547. doi:10.1016/j.fusengdes.2005.08.031.

[64] L.M. Toth, Containers for Molten Flouride Spectroscopy, Oak Ridge, TN, n.d.

[65] L.M. Toth, J.P. Young, G.P. Smith, Diamond-Windowed Cell for Spectrophotometry of Molten Fluoride Salts, Anal. Chem. 41 (1969) 683–685.

[66] Y.H. Cho, T.J. Kim, I.K. Choi, K.Y. Jee, Spectroscopic Approach for Studying the Lanthanide Ions in Molten Salt Media : UV-VIS , EPR and Luminescence Study, in: Korean Nucl. Soc. Autumn Meet., Korean Nuclear Society, Busan, Korea, 2005.

[67] A.L. Jurovitzki, M. Simpson, Monitoring Pyroprocessing vis UV-Vis Absoprtion Spectroscopy, in: Int. Pyroprocessing Res. Conf., Idaho Falls, ID, 2014.

[68] J.P. Young, J.C. White, A High-Temperature Cell Assembly for Spectrophotometric Studies of Molten Fluoride Salts, Anal. Chem. 31 (1959) 1892–1895.

[69] OSHA, Occupational Exposure to Beryllium, 2017.

[70] Department of Energy, Chronic Beryllium Disease Prevention Program, 2016.

[71] W.H. Jordan, S.J. Cromer, A.J. Miller, A W Savolainen, Aircraft Nuclear Propulsion Project Quarterly Progress Reportfor Period Ending December 10, 1955, Oak Ridge, TN, 1956.